NON-LINEAR TORSIONAL DYNAMIC ANALYSIS OF HYPOID GEAR PAIRS

by

XIN JIANG

A THESIS

Submitted in partial fulfillment of the requirements
for the degree of Master of Science in the
Department of Mechanical Engineering
in the Graduate School of
The University of Alabama

TUSCALOOSA, ALABAMA

2002

Submitted by Xin Jiang in partial fulfillment of the requirements for the degree of Master of Science specializing in Mechanical Engineering.

Accepted on behalf of the Faculty of the Graduate School by the thesis committee:

[redacted]
Bell-San Chen, Ph.D.

[redacted]
W. Steve Shepard, Ph.D.

[redacted]
Teik C. Lim, Ph.D.
Chairperson

[redacted]
Stuart R. Bell, Ph.D.
Department Chairperson

5-17-02
Date

[redacted]
Ronald W. Rogers, Ph.D.
Dean of the Graduate School

7/17/02
Date

LIST OF ABBREVIATIONS

DOF	degree of freedom
DTE	dynamic transmission error
HBM	harmonic balance method
NLTV	non-linear time-varying model
LTI	linear time-invariant model
LTV	linear time-varying model
CAPP	contact analysis program package

LIST OF SYMBOLS

I_1	rotary inertia of pinion
I_2	rotary inertia of gear
c_m	viscous damping coefficient
μ	coulomb friction coefficient
b	half of tooth-to-tooth backlash
T_1	torque on pinion
T_2	torque on gear
k(t)	time-varying gear mesh stiffness
e_0	static transmission error
δ_d	dynamic transmission error
λ_l	the directional rotation radius about the nominal rotation axis
τ_l	friction radius
$f(\delta_d + e_0)$	non-linear elastic mesh force
S_l	coordinate system (l=1,2 for pinion and gear respectively)
$\vec{i}_l$, $\vec{j}_l$	the triad of unit vectors that defines the coordinate system S_l
$\vec{\mathbf{n}}_l$	the unit normal vector of mesh point
$\vec{\mathbf{v}}_l$	the relative sliding velocity
$\vec{r}_l$	position vector of mesh point

$\tilde{T}_1$	normalized force on pinion
$\tilde{T}_2$	normalized force on gear
q_1	normalized transitional displacement of pinion
q_2	normalized transitional displacement of gear
m_m	equivalent mass of the gear pair
ω_n	natural frequency
ω_m	excitation mesh frequency
ω_l	angular velocity of pinion or gear
N_l	number of teeth of pinion (l=p) or gear (l=g)
Ω	normalized excitation frequency
ς	damping ratio
$\tilde{e}_0$	normalized static transmission error
$\tilde{\delta}_d$	normalized dynamic transmission error
$\tilde{k}(t)$	normalized mesh stiffness
k_m	mean value of mesh stiffness
k_a	percent variation of mesh stiffness
$\tilde{\lambda}_l$	normalized rotation radius
λ_m	mean value of rotation radius
λ_a	percent variation of rotation radius
$\tilde{\delta}$	normalized transmission error displacement

$\tilde{\delta}_m$	mean component of transmission error
$\tilde{\delta}_a$	alternating component of transmission error
$f(\tilde{\delta})$	normalized non-linear mesh force

Subscripts

l (l=1,2)	labels for pinion and gear respectively
m	labels for the mean value of time-varying parameters
a	labels for the oscillating part of time-varying parameters

ACKNOWLEDGMENTS

My most sincere gratitude goes to Dr. Teik C. Lim, who served as the Chair of my Master of Science thesis committee and academic adviser. His degree of support, encouragement, and excellent guidance throughout my entire graduate study at The University of Alabama, Tuscaloosa is the key to the success of this research project.

I would also like to express my sincere appreciation to Drs. W. Steve Shepard and Den-San Chen, who served as my committee members, for their valuable time used in reviewing and commenting on my thesis. Their suggestions and instructions helped elevate the thesis to a level of higher quality.

I would like to thank Dr. Hongbin Wang, who is also working on the hypoid gear project, for his technical assistance, suggestions, and advice.

The work presented in this thesis is based upon work partly supported by the National Science Foundation under Grant No. 9978581.

I am also thankful to the staff, professors, and the fellows in the research group at The University of Alabama for their friendship and helpings along months of the completion of my thesis research.

Last, but as important, I would like to dedicate the success of this thesis project to my magnificent parents and sister for their unconditional love, support, and understanding: Li-gui Jiang, Jin-mei Han, and Hong Jiang.

TABLE OF CONTENTS

LIST OF ABBREVIATIONS iii

LIST OF SYMBOLS viii

ACKNOWLEDGMENTS vii

LIST OF TABLES x

LIST OF FIGURES xi

ABSTRACT xv

CHAPTER Page

1. INTRODUCTION 1

2. LITERATURE REVIEW 4

3. DYNAMIC FORMULATION 10

3.1 Physical Model 10

3.2 Scope and Objectives 16

4. NUMERICAL SIMULATION 17

4.1 Comparison of Non-linear Response to Linear Theory 17

4.2 Parametric Studies 25

5. OUT-OF-PHASE TORSION MODE 31

5.1 Analytical Solutions 31

5.2 Comparison of Analytical and Numerical Solutions 39

6. NON-LINEAR GEAR DYNAMIC RESPONSE.....43

6.1 Response of Light Load Cases..... 43

6.2 Classification of Steady-State Solutions.....47

7. CONCLUSIONS AND RECOMMENDATIONS FOR FUTURE WORK.....55

7.1 Concluding Remarks.....55

7.2 Recommendations for Future Work.....56

REFERENCES 57

APPENDIXES

A. THE FLOW CHART OF THE RUNGE-KUTTA INTEGRATION SCHEME..... 60

B. MESH VECTORS DATA FROM CONTACT SIMULATION APPLYING CAPP 61

LIST OF TABLES

Table Page

1: Baseline System Parameters.....18

2: Normalized Force with Corresponding Actual Load.....19

LIST OF FIGURES

Figure Page

1. Torsional vibration model of a hypoid gear set.....12

2. Non-linear elastic mesh force due to backlash.....12

3. Illustration of double, single, and no tooth impact cases.....20

4. System response for load=0.4, $\tilde{e}_0 = 0.5, \varsigma = 0.08, k_a = 0.008$ (a) non-linear; (b) linear. 21

5. System response for load=0.8, $\tilde{e}_0 = 0.5, \varsigma = 0.08, k_a = 0.008$ (a) non-linear; (b) linear.....22

6. System response for load=1.6, $\tilde{e}_0 = 0.5, \varsigma = 0.08, k_a = 0.008$ (a) non-linear; (b) linear.....23

7. System response for load=3.2, $\tilde{e}_0 = 0.5, \varsigma = 0.08, k_a = 0.008$ (a) non-linear; (b) linear.....24

8. Frequency response $\tilde{\delta}_a$ for various input load levels for $\tilde{e}_0 = 0.5$, $\varsigma = 0.08$, $k_a = 0.008$: (a) T_l=0.1; (b) T_l=0.4; (c) T_l=0.8. 27

9. Frequency response for various mesh stiffness variation k_a levels for T_1=0.4, $\tilde{e}_0 = 0.5$, $\varsigma = 0.08$: (a) $k_a = 0.008$; (b) $k_a = 0.08$; (c) $k_a = 0.3$ 28

10. Frequency response for various damping ratio ς with T_1=0.1, $\tilde{e}_0 = 0.5$, $k_a = 0.008$: (a) $\varsigma = 0.04$ (b) $\varsigma = 0.08$; (c) $\varsigma = 0.12$ 29

11. Frequency response for various mesh vector characteristics with T_1=0.1, $\tilde{e}_0 = 0.5$, $k_a = 0.008$: (a) time-invariant mesh vectors; (b) simplified time-varying mesh vectors; (c) time-varying mesh vectors calculated from contact simulation applying CAPP.....30

12. Rigid body and flexible torsional modes of the hypoid gear pair.....32

13. Comparison of analytical results (□, ○, ▽) with numerical simulation (✳, ×,+) for T_1=0.1, $\tilde{e}_0$=0.75, $\varsigma = 0.08$, $k_a = 0.008$: (a) $\tilde{\delta}_a$ versus Ω; (b) $\tilde{\delta}_m$ versus Ω 40

14. Comparison of analytical results (□, ○, ▽) with numerical simulation (✳, ×,+) for T_1=0.4, $\tilde{e}_0$=0.5, $\varsigma = 0.08$, $k_a = 0.008$: (a) $\tilde{\delta}_a$ versus Ω; (b) $\tilde{\delta}_m$ versus Ω 41

15. Comparison of analytical results (□, ○, ▽) with numerical simulation (✳, ×,+) for T_1=0.8, $\tilde{e}_0$=0.5, $\varsigma = 0.08$, $k_a = 0.008$: (a) $\tilde{\delta}_a$ versus Ω; (b) $\tilde{\delta}_m$ versus Ω 42

16. Frequency response of baseline system for mean load T_1=0.1 $\tilde{e}_0$=0.5 $k_a = 0.008$ 44

17. Time history of system steady-state response for $\Omega = 0.625$ 45

18. Time history of system steady-state response for $\Omega = 0.65$.....45

19. Time history of system steady-state response for $\Omega = 0.675$.....46

20. Time history of system steady-state response for $\Omega = 0.7$.....46

21. A period-one harmonic response for baseline case, $\Omega = 0.65$; (a) phase plane; (b) Poincare map; (c) time history; (d) FFT spectra.....49

22. A period-two sub-harmonic response for baseline case, $\Omega = 1.0$; (a) phase plane; (b) Poincare map; (c) time history; (d) FFT spectra.....50

23. A period-two sub-harmonic response for baseline case, $\Omega = 1.3$; (a) phase plane; (b) Poincare map; (c) time history; (d) FFT spectra.....51

24. A period-four sub-harmonic response for baseline case, $\Omega = 1.4$; (a) phase plane; (b) Poincare map; (c) time history; (d) FFT spectra.....52

25. A chaotic response for baseline case, $\Omega = 1.6$; (a) phase plane; (b) Poincare map; (c) time history; (d) FFT spectra.....53

26. A period-two sub-harmonic response for baseline case, $\Omega = 1.8$; (a) phase plane; (b) Poincare map; (c) time history; (d) FFT spectra.....54

ABSTRACT

High-speed right-angle geared rotor systems are widely used in automotive and rotorcraft transmission applications. Hypoid gear pairs are one of the commonly applied right-angle geared systems. They are designed to transmit significant amount of rotational power between two perpendicular, non-intersecting shafts. However, this class of geared rotor systems is often plagued by excessive vibration and noise problems. In most cases, the gear whine generated leads to costly warranty issues. This thesis work is focused on the dynamic response analysis of a generic hypoid gear pair. A unique non-linear time-varying dynamic model of the hypoid gear pair system is proposed which includes backlash non-linearity, linear time-varying gear meshing stiffness, time-varying mesh characteristic vectors as well as sliding friction effects. The model is applied to study the physical phenomenon governing the generation of dynamic mesh force that is believed to be the main cause of high vibration and noise levels. Solutions are presented in the forms of semi-analytical and numerical integration results. Parametric studies reveal new, previously unstudied findings of the controlling factors and vibratory behaviors under light, medium, and high mean loads. Using the numerical simulation, critical non-linear behaviors in system response such as the jump phenomenon, impact regimes, sub-harmonic, and chaotic resonance are investigated. Classification of the steady-state solutions is presented based on the results of time histories, phase plane plots, Poincare maps, and Fourier spectra.

CHAPTER 1

INTRODUCTION

The hypoid gear set is widely used in the rear axles of trucks and passenger cars to transmit motion in perpendicular non-intersecting directions. The gears in this application are often subjected to a harmful dynamic response that can cause gear whine annoyance and structural fatigue problems. To date many of these kinds of chronic axle-drive noise problems seen in automotive systems continue to persist due to the lack of a comprehensive way to deal with the design concern effectively. Previous research activities are mostly directed toward the reduction of transmission error and optimization of tooth contact bearing patterns. However, it has been realized that some axle gear noise problems are not only caused by the quality of the gear design and manufacturing parameters, but also resulted from the structural resonance behavior and sensitivity of the driveline system response to transmission error excitation. In order to develop a better understanding of hypoid gear noise generation and transmission problems, an in-depth investigation on the torsional dynamics of the hypoid gears is performed in this thesis research.

This research is concerned with the torsional dynamic analysis of the hypoid gear system. A non-linear time-varying two degrees-of-freedom model is proposed and includes backlash non-linearity, time-varying mesh stiffness, line-of-action and contact point, and sliding friction effects. The mathematical formulations are presented to

characterize the system torsional motion. The frequency response characteristics of both linear and non-linear baseline systems are studied by using a numerical simulation technique. Semi-analytical solutions are constructed by the harmonic balance method (HBM) for the out-of-phase torsion mode and compared with numerical calculations. Parametric studies are performed to quantify the dependence of dynamic response to basic gear design parameters and operating conditions. For system non-linear behavior under a light load condition, different types of steady-state solutions are classified based on phase planes, Poincare maps, time histories, and FFT spectra. Non-linear behaviors in system torsional response like the jump phenomenon, impact regimes, sub-harmonic, and chaotic resonances are observed to be most acute under the light load condition. Hence, the intention of this study is to gain a better understanding of the underlying physics of the gear noise generation and transmission problems, and to determine the primary controlling design parameters. The ultimate goal is to provide hypoid gear users with a practical set of engineering analysis tools to design quieter products and increase the range of applications.

The organization of the rest of this report is given as follows:

Chapter 2 discusses through a literature review the limitations and salient features of available research work on the hypoid geared rotor systems. It also introduces the basic approaches used to deal with gear vibration and noise problems. The existing study on non-linear vibro-impact problems in parallel axis gear pair is examined for comparison. The discussion further clarifies the need for the theory of parallel axis case to be further refined for perpendicular axis case due to the unique nature of the hypoid geared rotor systems.

Chapter 3 proposes a non-linear time-varying two degrees-of-freedom dynamic model of hypoid gears, which can also be used for bevel gear by setting the offset to be zero. The analytical formulations are presented to characterize the system torsional dynamic motion. In the derivation, the backlash non-linearity, time-varying parameters and sliding friction effects are considered.

Chapter 4 presents the numerical simulation results of both non-linear and linear models based on a baseline system. System responses under different load levels are compared and three tooth impact cases in the presence of backlash are discussed.

Chapter 5 presents the study on the out-of-phase torsion mode. Semi-analytical solutions are constructed by using the harmonic balance method (HBM). The approximate analytical solutions are validated by comparing predictions with the results obtained by numerical simulation for various load cases.

Chapter 6 gives a further investigation of the non-linear phenomenon such as jump discontinuity, sub-harmonic, and chaotic solutions in lightly loaded system response. Classification of the steady-state solutions is presented based on time histories, phase plane, Poincare maps, and FFT spectra.

Chapter 7 provides a summary of the significant discovery of this research project and recommendations for future work. Appendix A gives a flow chart of the Runge-Kutta integration scheme used in obtaining the numerical solutions. Appendix B presents the time-varying mesh characteristic vectors obtained from contact analysis applying CAPP.

CHAPTER 2

LITERATURE REVIEW

The dynamic response of gears remains a paramount concern because of noise and dynamic loads generated. It has been the subject of numerous studies over the past few decades. There are essentially 2 basic approaches used to deal with gear vibration and noise problems. The classical, direct approach attempts to minimize transmission error excitation by optimizing gear tooth profile and manufacturing processes. Typical approaches include transmission error modeling and measurement, tooth stress and load calculations, and identification of mesh harmonics and sideband frequencies. Increasingly more gear research efforts have focused on a second approach involving system vibration and noise response modeling. This approach attempts to formulate the problem on the basis of tuning structural parameters to minimize undesirable vibro-acoustic response generation and transmission. Here, the effects of system dynamics can be modeled using time-invariant or time-varying, linear or non-linear models. In the last few decades, this system approach has been applied extensively to analyze parallel axis geared rotor system dynamics [1-8].

While parallel axis geared rotor system dynamics has been extensively investigated and its field is relatively mature, very little research work actually dealt with the prediction of dynamic response of right-angle geared rotor systems such as bevel and hypoid gear pairs. This lack of studies persists in spite of the fact that there have been

many instances of noisy applications using relatively high quality gears because of the contribution from the structural resonance effect. One of the reasons for this lack of research attention was the complexity of gear kinematics in right-angle drive train applications. Most of the research work related to bevel and hypoid gears is limited to the modeling of transmission error and the corresponding dynamic factor [9-12]. Studies related to right-angle geared rotor system dynamics have been primarily experimental in nature. Until more recently, the few modeling efforts attempted in the past were limited to crude, semi-empirical methods [13-17].

In recent years, a team led by Lim [18-22] began formulating mesh and dynamic models to study the dynamics of right-angle geared rotor systems. In particular, their studies focus on high-speed bevel and hypoid gears. In one of the studies done, Cheng and Lim [18] proposed a gear kinematic model based on the exact gear geometry to analyze the hypoid gear mesh-coupling mechanism. They applied this mesh-coupling theory to develop a 3-dimensional, multiple degrees-of-freedom, linear dynamic model of the hypoid gear pair. The model was applied to examine the effects of various gear parameters on vibratory characteristics of the hypoid geared rotor system. The single-point mesh-coupling concept was later extended to examine the effects of non-linear, time-varying mesh characteristic on translation-rotational dynamic response [21-22]. However, the study did not examine multiple solution regimes and only relied on numerical treatment. In contrast, this thesis formulates a lower order torsional dynamic model to examine the presence of non-linear, time-varying phenomena more in-depth.

The non-linear dynamic problem in spur or helical gears with gear backlash has been extensively studied by some researchers. There are generally four approaches in solving this class of the governing equations.

(i) Numerical integration methods. This method can readily solve large classes of non-linear dynamic problems. However in some situations, such as lightly damping system, the actual solutions near the jump frequencies depend on the choice of initial conditions. This method may become impractical when the computational expenses required to obtain steady-state solutions are high, especially for lightly damped systems.

(ii) Piecewise linear technique. This technique may be quite difficult to implement, especially with impacts that are not equally spaced. It is also limited by the requirement that the non-linearities are piecewise linear. If a non-linear contact stiffness or impact damping is included, this method will no longer be valid.

(iii) Analog simulation. This simulation technique is restricted by the size of the analog computer and availability of non-linear elements.

(iv) Single or multiple-term harmonic balance method (HBM). This method was first introduced by Bogolyubov and Krylov in the mid-1930s [23] for clearance type non-linearity. It is widely used in constructing analytical solutions and criteria for occurrence of tooth separation and back-collision. One limitation of the harmonic balance method is that the effects of initial conditions on the solution cannot be considered.

In this literature review, specific attentions are focused on the modeling of geared rotor systems with backlash non-linearity, and the analytical/computational methods used previously to analyze the vibro-impact problem. Some of the relevant studies are discussed below.

One of the earlier attempts in the study of vibro-impact problems was by Comparin and Singh [24]. They investigated the steady-state frequency response of a single degree-of-freedom impact pair with a clearance type non-linearity. The harmonic balance method was used to develop approximate analytical solutions to the equations of motion of a single impact pair including a general discussion of the existence and stability of these solutions. The results were validated using an analog computer simulation and it was reported that the use of numerical integration may lead to inaccurate results over certain frequency ranges.

In a subsequent study, Comparin and Singh [25] extended the single degree-of-freedom system to a multiple degrees-of-freedom (MDOF) system with clearances. The analysis represented an initial investigation into the dynamic behavior of MDOF geared rotor systems composed of coupled non-linear oscillators. The harmonic balance method was applied here for analytical analysis. Also, an analysis methodology for MDOF systems was introduced and illustrated for practical cases. The studies formed the basis for the development of simplified approximate solutions.

In another paper, Kahraman and Singh [5] investigated the non-linear frequency response characteristics of a single degree-of-freedom spur gear pair with backlash non-linearity and focused on the internal excitation of transmission error between the spur gear pair. The governing non-linear differential equation used was different from the

conventional formulation for clearance non-linearity or vibro-impact systems. Some key issues were discussed including the difference between internal and external excitations, existence of multiple impact regimes, chaotic phenomenon, and sub-harmonic resonances.

Kahraman and Singh [6] also examined the non-linear frequency response characteristics of a geared rotor-bearing system. A three degrees-of-freedom model was developed that included non-linearities associated with radial clearances in the radial rolling element bearings and backlash between a spur gear pair. Here, linear time-invariant gear meshing stiffness was assumed. Applicability of both analytical and numerical solution techniques to the MDOF non-linear problem was investigated. Satisfactory agreement was found between the theoretical predictions and available experimental data. Furthermore, a criterion used to classify the steady-state solutions was presented, and the conditions for chaotic, quasi-periodic, and sub-harmonic steady-state solutions were determined.

In a more recent work, Kahraman and Blankenship [26] demonstrated experimentally the existence of several forms of non-linear dynamic behaviors including the jump discontinuities, sub- and super-harmonic resonances, chaotic response, and multiple coexisting stable solutions. These observed behaviors are in fact consistent with the previous theoretical predictions from simple mechanical oscillators with clearance having combined parametric and forcing excitations.

In most of the above-mentioned models on gear dynamic analysis, it was assumed that the main sources of dynamic excitation in the pair gear systems occur along the line-of-action and are due to the time-varying tooth stiffness and static transmission error.

Recently, Vaishya and Singh [27] proposed a new gear dynamic model that incorporated non-linearity induced by sliding friction. Both non-linear time-varying (NLTV) system and linear time-varying (LTV) system were employed in their study. The physical phenomena associated with these two models were compared and the essential differences in the system behaviors were examined.

In spite of the fact that much is known about non-linear effects in parallel axis gears, their formulations are not directly applicable to right-angle cases due to the unique nature of meshing behavior in this class of gears. The meshing position and normal force vectors in hypoid gears are time and spatial varying. Moreover, the friction force generated at the mesh interface gives rise to 3-dimensional oblique force and moment reactions on the gear members, which may lead to internal parametric excitation. Gear backlash resulting in clearance type non-linearity at the mesh can lead to tooth separation or back-side collision. An in-depth dynamic analysis is needed to address these issues and to examine the importance of these effects. The approaches used in parallel axis gears must be modified to make it more applicable to right-angle cases.

CHAPTER 3

DYNAMIC FORMULATION

In parallel axis gears, the line-of-action is generally time-invariant, as defined by the pressure and helix angles, because the normal vectors at the theoretical contact points of each pair of teeth in mesh are co-linear. However, this is not the case in hypoid gears. Due to the inherent hypoid tooth geometry, the resultant mesh force vector varies as the hypoid gears rotate over the mesh cycle. This is due to the fact that the normal lines-of-action of each pair of teeth in contact are neither co-linear nor parallel. This produces a net force transmission that oscillates with a periodicity equal to the meshing angle. Similar effects can be expected from the resultant friction excitation that also behaves periodically. It is widely accepted that the transmission error excitation is the major source of gear whine noise, which is also the primary focus here. This chapter deals with the development of a mathematical model for hypoid gears with backlash non-linearity. The transmission error is assumed to be the primary source of excitation.

3.1. Physical Model

A two degrees-of-freedom torsional vibration model of a hypoid gear pair shown in Figure 1 is considered to investigate the system steady state frequency response. This dynamic model that only simulates the rotational response is used to analyze the out-of-phase gear pair torsional mode without other complicating effects. It is applicable to early concept design phase where the rest of the drive train system is not yet defined precisely.

Time-varying mesh vectors, time-varying mesh stiffness, sliding friction effects, transmission error excitation, and backlash non-linearity will be incorporated into the derivation.

The equations of torsional motion of the gear pair as shown in Figure 1 are

$$I_1\ddot{\theta}_1 - (\lambda_1 - \mu\tau_1)c_m(\dot{\delta}_d + \dot{e}_0) - (\lambda_1 - \mu\tau_1)f(\delta_d + e_0)\cdot k(t) = T_1, \tag{1a}$$

$$I_2\ddot{\theta}_2 + (\lambda_2 + \mu\tau_2)c_m(\dot{\delta}_d + \dot{e}_0) + (\lambda_2 + \mu\tau_2)f(\delta_d + e_0)\cdot k(t) = -T_2. \tag{1b}$$

The numerical subscripts of 1 and 2 are used to designate the reference to the pinion and gear, respectively, I_1 and I_2 are rotary inertias, c_m is the viscous damping coefficient, μ is the coulomb friction coefficient, $e_0(t)$ is the static transmission error, T_1 and T_2 are torques applied to the pinion and gear respectively, and k(t) is the linear time-varying gear mesh stiffness. The dynamic transmission error is defined as $\delta_d = \lambda_2\theta_2 - \lambda_1\theta_1$, while the directional rotation radius is $\lambda_l = \vec{\mathbf{n}}_l \cdot (\vec{i}_l \times \vec{r}_l)$ (l=1,2 for pinion and gear, respectively), and the radial vector of the friction load is $\tau_l = \vec{\mathbf{v}}_l \cdot (\vec{j}_l \times \vec{r}_l)$ similar to the gear mesh model developed by Cheng and Lim [18]. Here, $\vec{i}_l$ and $\vec{j}_l$ are the triads of unit vectors that define the coordinate systems for pinion and gear, $\vec{\mathbf{n}}_l$ is the unit normal vector of mesh point, $\vec{\mathbf{v}}_l$ is the relative sliding velocity, and $\vec{r}_l$ is the position vector of mesh point. Here, the non-linear displacement term $f(\delta_d + e_0)$ is a clearance-type backlash function as shown in Figure 2,

$$f(\delta_d + e_0) = \begin{cases} \delta_d + e_0 - b, & \delta_d + e_0 \geq b \\ 0, & -b < \delta_d + e_0 < b \\ \delta_d + e_0 + b, & \delta_d + e_0 \leq -b \end{cases}. \tag{2}$$

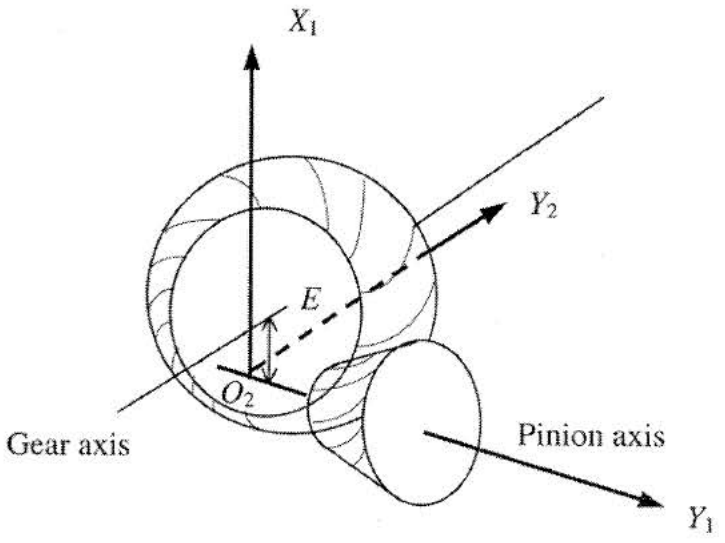

Figure 1. Torsional vibration model of a hypoid gear set.

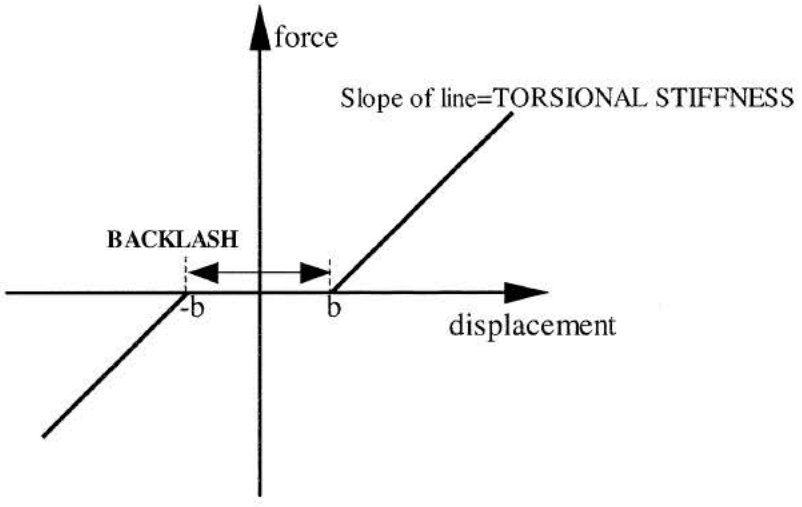

Figure 2. Non-linear elastic mesh force due to backlash.

Most gear pairs generally contain a certain degree of backlash in order to achieve better lubrication and eliminate interference. However, the presence of backlash may induce tooth separation and impacts in unloaded or lightly loaded geared drives. Such impacts typically cause excessive vibration and noise problems, and larger dynamic loads that negatively affect durability. Gear backlash non-linearity is essentially a discontinuous and piecewise differentiable function. It represents a strong non-linear interaction controlling the governing differential equations.

There are two types of excitation mechanism for geared rotor systems namely the external and internal dynamic loads. (a) External excitations. This group includes excitations due to rotating mass imbalances, geometric eccentricities, and prime mover and/or load torque fluctuations. Although mass imbalances and geometric eccentricities can be reduced though improved design and manufacturing, torque fluctuations are not easy to eliminate since they are determined by the characteristics of the prime mover (piston energies, DC motors, etc.) and load. Such excitations typically occur at low frequencies, which are the first few multiples of the input shaft speed. Practical examples include rattle problems in lightly loaded automotive transmissions and machine tools. (b) Internal excitations. This group includes high frequency excitations caused by the manufacturing related profile and spacing errors, and the elastic deformation of the teeth, shafts and bearings. Under the static conditions, the combined effects of such mechanisms yield the overall kinematic error function known as the static transmission error denoted by $e_0(t)$. This error is defined as the difference between the actual angular position of the driven gear and where it would be if the gears were perfect. In gear dynamic models, $e_0(t)$ is modeled as a periodic displacement excitation at the mesh point

along the line-of-action and its period is given by the fundamental meshing frequency. Problems arising from this form of excitation include gear noise and vibration in automotive, aerospace, industrial, marine and appliance geared systems. In the formulation of the hypoid gear pair, the high frequency internal excitation due to the static transmission error $e_0(t)$ is considered, while the low-frequency external excitation due to torque fluctuation is neglected, i.e., T_1 and T_2 are assumed constant.

To simplify the analytical and digital simulations, and to provide generality, the above equations of motion are made dimensionless. Equation (1) can be transformed into a dimensionless form by assuming

$$q_l = \lambda_l \theta_l / b \,,\ l=1,2 \tag{3}$$

$$v_l = (\frac{\lambda_l - \mu\tau_l}{I_l})\lambda_{lm} m_m, \tag{4}$$

$$\varsigma = \frac{1}{2} c_m /(m_m \omega_n), \tag{5}$$

$$m_m = \left[(\lambda_{1m}^2 - \mu\tau_{1m}\lambda_{1m})/I_1 + (\lambda_{2m}^2 + \mu\tau_{2m}\lambda_{2m})/I_2\right]^{-1}. \tag{6}$$

The natural frequency is $\omega_n = \sqrt{k_m / m_m}$, and the excitation mesh frequency ω_m is given by $\omega_m = N_l \cdot \omega_l$, where N_l is the number of teeth on the pinion (l=1) or gear (l=2), and ω_l is the angular velocity of pinion or gear. In the dimensionless form of the governing equations, the fundamental excitation frequency of transmission error is $\Omega = \omega_m / \omega_n$, while its dimensionless amplitude is $\tilde{e}_0 = e_0 / b$. The transmission error excitation is represented in the form of $\tilde{e}_0(t) = \tilde{e}_0 \sin(\Omega\tau + \phi)$. Furthermore, let

$$\tilde{k}(t) = k(t)/k_m = 1 + k_a, \tag{7}$$

$$\tilde{\lambda}_l = \lambda_l / \lambda_{lm} = 1 + \lambda_{la}, \tag{8}$$

$$\tilde{T}_l = T_l m_m / (b k_m I_1) \cdot \lambda_{lm}, \tag{9}$$

$$\tilde{\delta} = (1 + \lambda_{2a}) q_2 - (1 + \lambda_{1a}) q_1 + \tilde{e}_0. \tag{10}$$

The resulting governing equations of motion in dimensionless form become

$$\ddot{q}_1 - 2\varsigma \dot{\tilde{\delta}} \nu_1 - f(\tilde{\delta}) \nu_1 \tilde{k}(t) = \tilde{T}_1, \tag{11a}$$

$$\ddot{q}_2 + 2\varsigma \dot{\tilde{\delta}} \nu_2 + f(\tilde{\delta}) \nu_2 \tilde{k}(t) = -\tilde{T}_2, \tag{11b}$$

$$f(\tilde{\delta}) = \begin{cases} \tilde{\delta} - 1, & \tilde{\delta} > 1 \\ 0, & -1 \le \tilde{\delta} \le 1 \\ \tilde{\delta} + 1, & \tilde{\delta} < -1 \end{cases}. \tag{12}$$

In the case of the time-varying parameters, the Taylor series can be used to expand $\nu_l, \tilde{k}(t)$, and $\tilde{\lambda}_l(t)$. For a given gear pair with constant rotational velocity, these parameters are periodic excitations whose periodicity is the same as the mesh frequency of the transmission error $\tilde{e}_0(t)$. The periodic parameters are represented in the form of

$$\nu_l = \nu_{lm} + \nu_{la} \sin(\Omega \tau + \varphi_l), \tag{13a}$$

$$\nu_{1m} + \nu_{2m} = 1, \tag{13b}$$

$$\tilde{k}(t) = 1 + k_a \sin(\Omega \tau + \psi_k), \tag{14}$$

$$\tilde{\lambda}_l(t) = 1 + \lambda_{la} \sin(\Omega \tau + \alpha_l). \tag{15}$$

Note that only the component of fundamental frequency is considered, and all the higher excitation harmonics are neglected in the expansion. Also, $\tilde{T}_1$ and $\tilde{T}_2$ are assumed constant such that no external torque fluctuation is present.

3.2. Scope and Objectives

Equation (11) represents the dynamics of hypoid gear pair with backlash as excited harmonically by the transmission error excitation $\tilde{e}_0(t)$. In fact, the study of the dynamic behavior of the hypoid gear pair essentially reduces to an analysis of the steady-state frequency response characteristics of Equation (11). The goals here are to perform an in-depth study of the dynamic characteristics of the harmful out-of-phase gear pair torsional mode, and to analyze the critical controlling design parameters. Specific objectives are given as follows:

1. Compare the frequency responses of linear and non-linear systems by using numerical simulation techniques.
2. Construct analytical solutions for the out-of-phase torsion mode by using the harmonic balance method, and compare the analytical solutions with numerical simulation results.
3. Perform parametric studies to understand the effects of several system controlling parameters on system response.
4. Investigate the non-linear system response characteristics by using numerical simulation in order to understand the occurrence of certain critical non-linear behaviors like the jump phenomenon, multiple solutions, sub-harmonic and chaotic solutions.
5. Examine steady-state solutions based on numerical results in the effort to understand the characteristics of the response over the operating frequency range.

CHAPTER 4

NUMERICAL SIMULATION

4.1. Comparison of Non-linear Response to Linear Theory

In this section, a numerical simulation technique is applied to compare the system frequency response characteristics for the non-linear time-varying model and the linear time-invariant model. The linear time-invariant model can be obtained by neglecting time-varying parameters and non-linear effects. The resulting linearized governing equations of motion are given by

$$I_1\ddot{\theta}_1 - (\lambda_{1m} - \mu\tau_1)c_m\dot{\delta}_d - (\lambda_{1m} - \mu\tau_1)\delta_d \cdot k_m = T_1, \tag{16a}$$

$$I_2\ddot{\theta}_2 + (\lambda_{2m} + \mu\tau_2)c_m\dot{\delta}_d + (\lambda_{2m} + \mu\tau_2)\delta_d \cdot k_m = -T_2. \tag{16b}$$

This formulation relies on the assumption of an effective pitch point location. Here, the dynamic transmission error (DTE) is expressed as $\delta_d = \lambda_{2m}\theta_2 - \lambda_{1m}\theta_1$.

Table 1 shows the basic gear design parameters and operating conditions used in the baseline study. Numerical simulation is performed by varying a set of realistic data to compare the response of the non-linear model with the linear theory. To determine a practical baseline value of the drive torque, a transformation equation is used:

$$T_{1g} = \tilde{T}_{1g} bk_m I_1 /(m_m \lambda_{1m}). \tag{17}$$

From the baseline parameters specified in Table 1 and Equation (17), the actual loads and corresponding normalized forces are obtained as listed in Table 2.

Table 1.

Baseline System Parameters

Parameters	Magnitude
Coulomb friction coefficient, μ	0.05
Damping ratio, ς	0.08
Mean mesh vector of the pinion, v_{1m}	0.3
Mean mesh vector of the gear, v_{2m}	0.7
Variation amplitude of pinion mesh vector, v_{1a}	0.00015
Variation amplitude of gear mesh vector, v_{2a}	0.00057
Mean directional rotation radius of the pinion, λ_{1m} (m)	0.0762
Mean directional rotation radius of the pinion, λ_{2m} (m)	0.18834
Variation amplitude of pinion directional rotation radius, λ_{1a}	0.0005
Variation amplitude of gear directional rotation radius, λ_{2a}	0.00075
Transmission error excitation, $\tilde{e}_0$	0.5
Backlash, $2b$ (μm)	10
Mean mesh stiffness, k_m (N/m)	$2*10^6$
Variation amplitude of mesh stiffness, k_a	0.08
Rotary inertia of pinion, I_1 (kg-m^2)	0.13
Rotary inertia of gear, I_2 (kg-m^2)	1.4188

Table 2.

Normalized Force with Corresponding Actual Load

Normalized force	Actual load (lbf-in)
0.4	649.32
0.8	1298.64
1.6	2597.29
3.2	5194.57

The governing non-linear differential Equation (11) is numerically solved by using 5^{th}-6^{th} order, variable step Runge-Kutta numerical integration routine that is suitable for strong non-linear cases. Due to gear backlash, the torsional vibration can result in relative motion across the clearance space and impacts between the adjacent teeth. Thus, tooth separation may occur in lightly loaded geared drives. There are three cases for which solutions can be obtained: (a) no impacts (no tooth separation); (b) single-sided impacts (tooth separation, but no back collision); (c) two-sided impacts (back collision). Figure 3 is an illustration of these 3 tooth impact regions. The conditions for no impacts, single-sided impacts and double-sided impacts are also influenced by the input mean load. In the numerical simulation results, the actual impact conditions will be monitored.

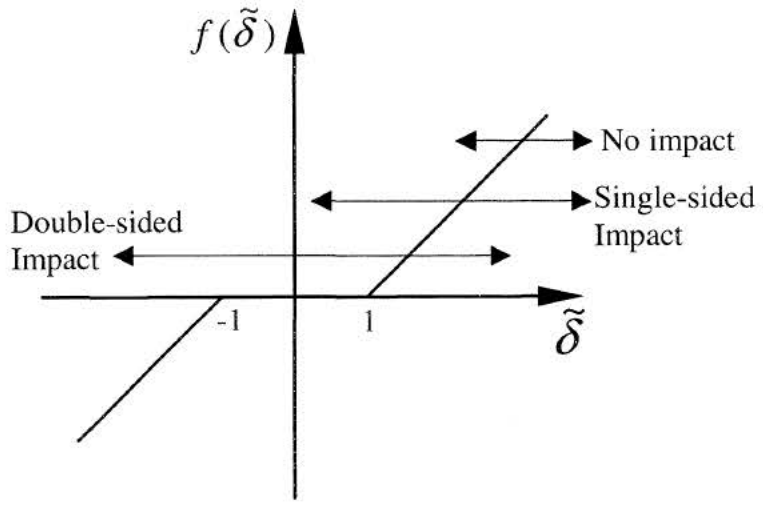

Figure 3. Illustration of double, single, and no tooth impact cases.

It is generally known that input mean load is one of the key parameters for determining the resultant tooth impact region and system non-linear response. The numerical simulation results given in Figures 4-7 are used to show direct comparisons of the non-linear and linear response spectra for various load levels. Significant differences are observed between the non-linear and linear results at light load condition as shown in Figure 4. As load increases, the non-linear response converges much closer to the linear characteristic even though the peak magnitudes of both cases are still slightly different as shown in Figure 7. The difference in magnitudes is attributed to damping, friction, and other non-linear time-varying effects present. In the light load case, non-linear behaviors like jump phenomenon, single and double sided impacts, sub-harmonic, and chaotic responses are observed. Another unique characteristic of the non-linear response is the difference between the increasing rotational speed response and decreasing one due to the effects of non-linearity and time-variation characteristics.

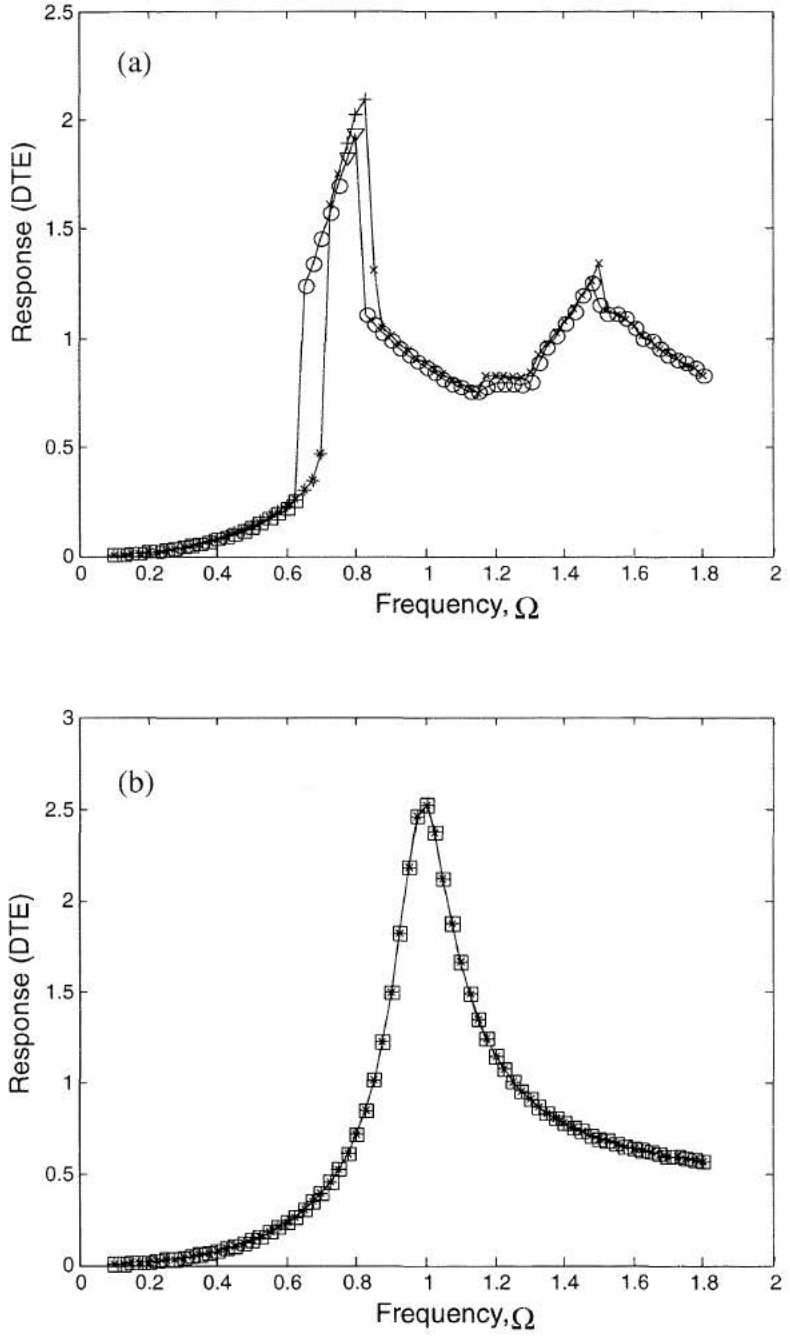

Figure 4. System response for load=0.4, $\tilde{e}_0 = 0.5, \varsigma = 0.08, k_a = 0.008$ (a) non-linear; (b) linear. (Keys: $\ast, \times$, + represent response for increasing frequency; $\triangledown$, O, $\square$ represent response for decreasing frequency; $\square$, $\ast$, no impact; O, $\times$, single sided impact; $\triangledown$, +, double-sided impact).

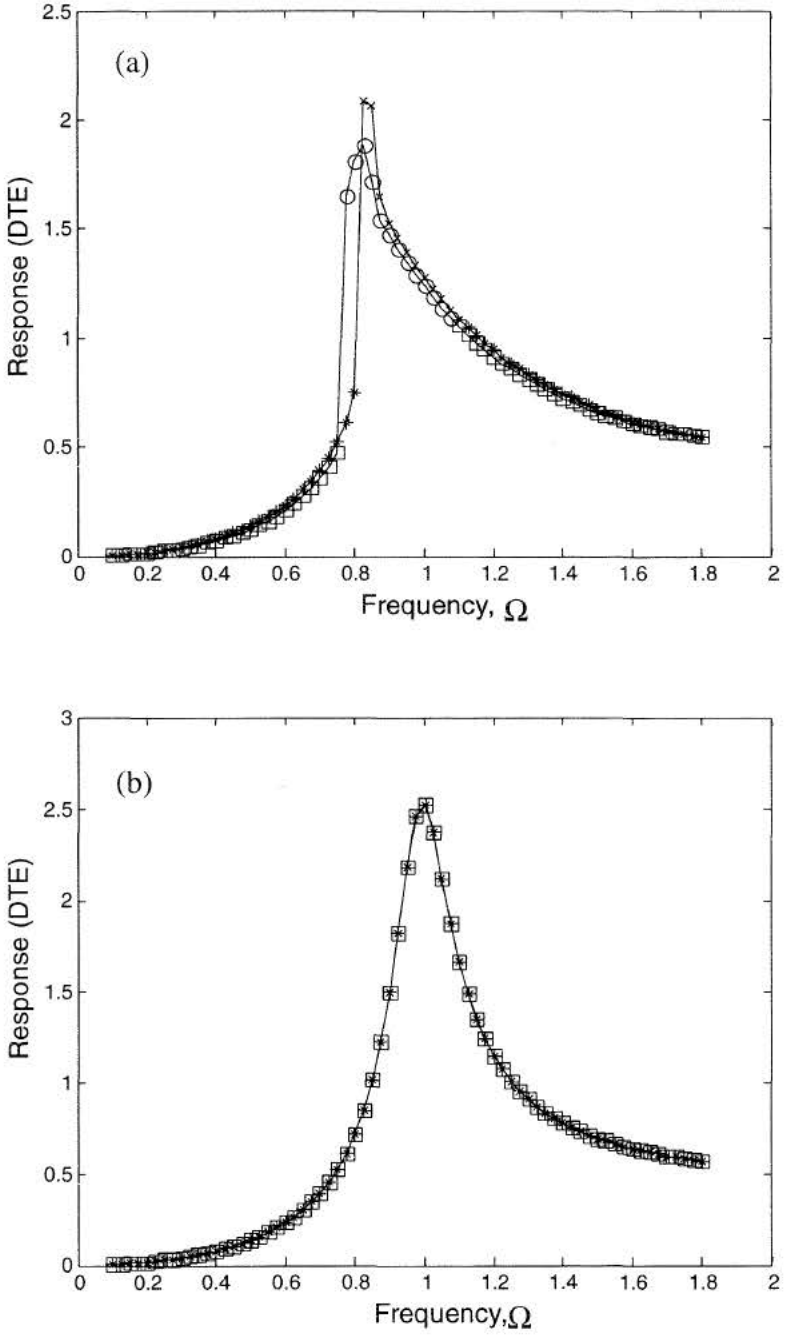

Figure 5. System response for load=0.8, $\tilde{e}_0 = 0.5, \varsigma = 0.08, k_a = 0.008$ (a) non-linear; (b) linear. (Keys: $\ast, \times$, + represent response for increasing frequency; $\triangledown$, O, $\square$ represent response for decreasing frequency; $\square$, $\ast$, no impact; O, $\times$, single sided impact; $\triangledown$, +, double-sided impact).

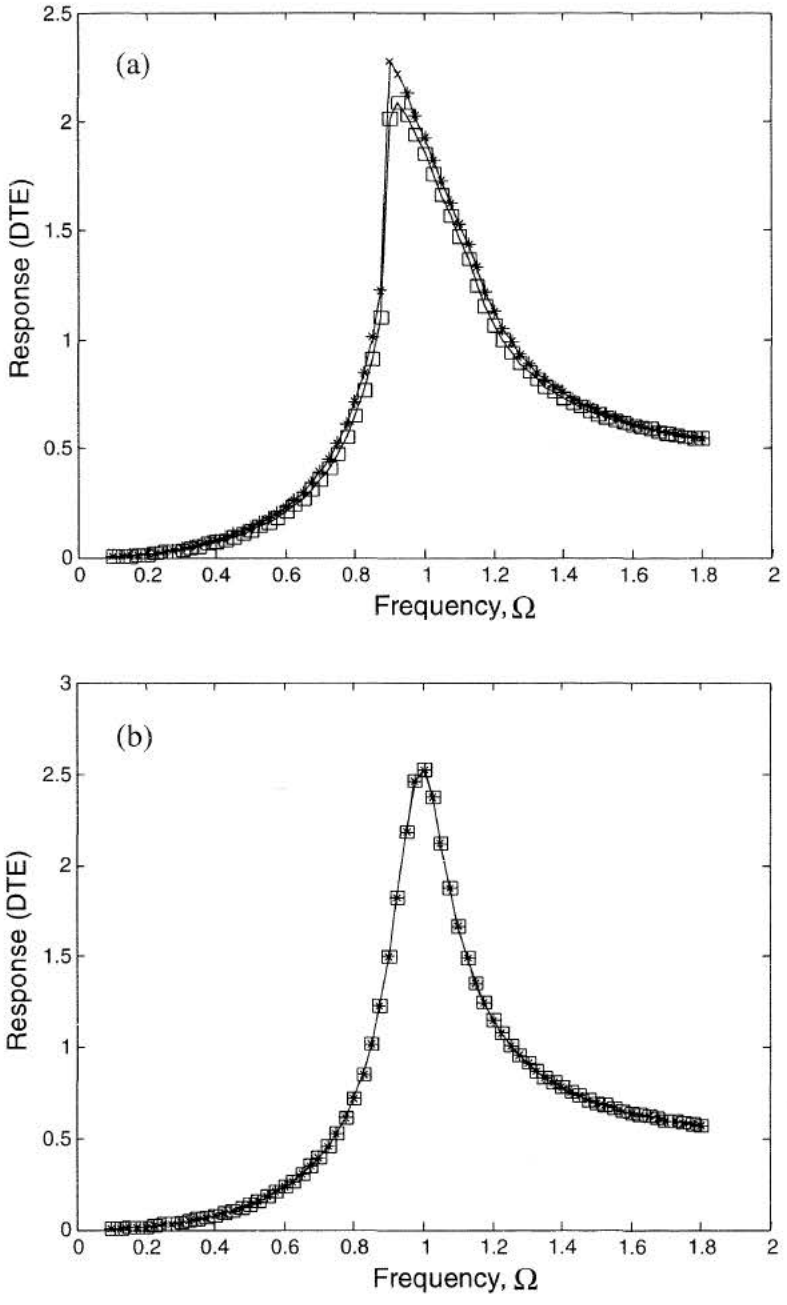

Figure 6. System response for load=1.6, $\tilde{e}_0 = 0.5, \varsigma = 0.08, k_a = 0.008$ (a) non-linear; (b) linear. (Keys: $*, \times$, + represent response for increasing frequency; ∇, O, $\square$ represent response for decreasing frequency; $\square$, $*$, no impact; $O, \times$, single sided impact; ∇, +, double-sided impact).

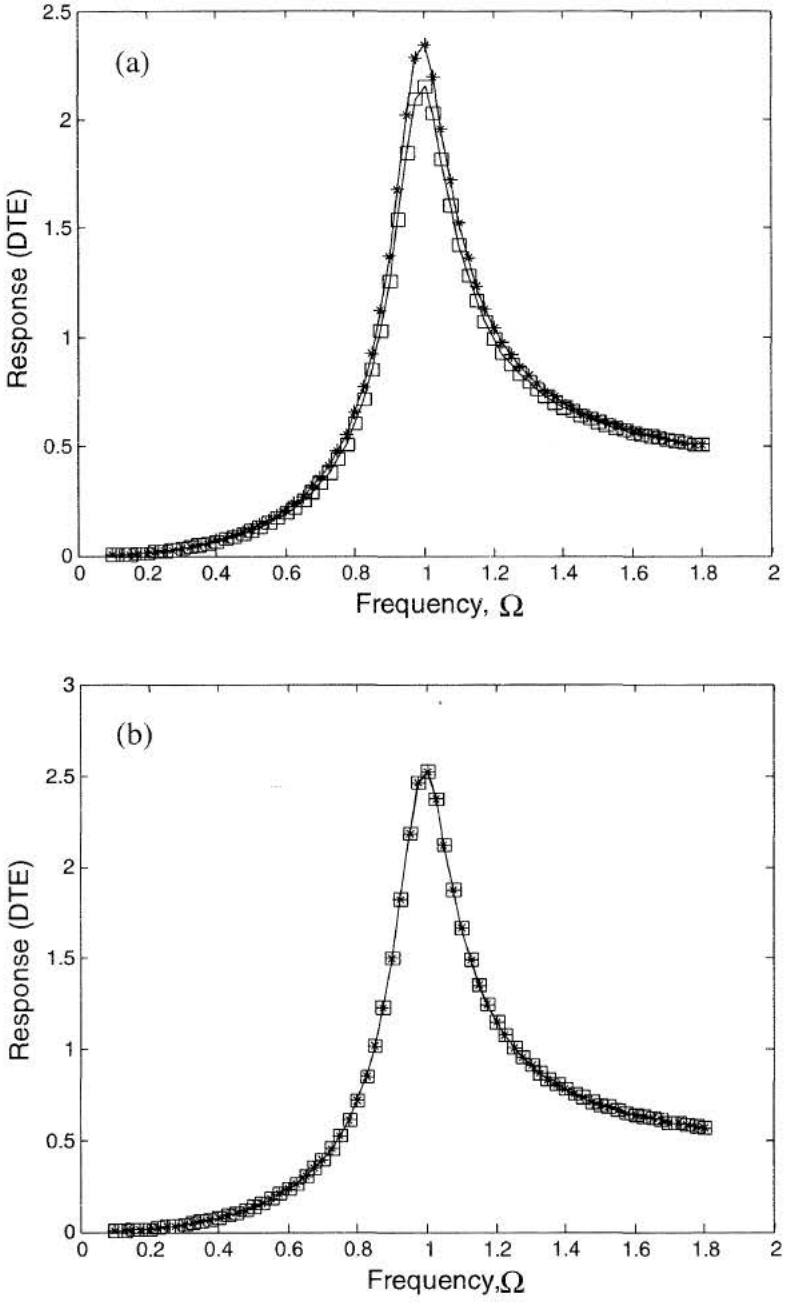

Figure 7. System response for load=3.2, $\tilde{e}_0 = 0.5, \varsigma = 0.08, k_a = 0.008$ (a) non-linear; (b) linear. (Keys: $\ast, \times$, + represent response for increasing frequency; $\bigtriangledown$, O, $\square$ represent response for decreasing frequency; $\square$, $\ast$, no impact; $\mathrm{O}, \times$, single sided impact; $\bigtriangledown$, +, double-sided impact).

4.2. Parametric Studies

A set of parametric studies is performed using numerical simulation technique to examine the effects of several system parameters. First, the effect of input load T_I is examined. Results for three T_I levels are compared in Figure 8 in which one can see clearly that the variation in frequency response amplitudes, transition frequencies, and the existence of various impact regimes depend on the input load. For the light load case as shown in Figure 8(a), typical non-linear behaviors such as jump phenomenon, tooth impacts, sub-harmonic and chaotic solutions are clearly observed. However, for the mid-load case as shown in Figure 8(b), the system behavior becomes more predictable and only a small region around the resonant frequency is dictated by the single-sided impacts. However, sudden discontinuity is still observed. When T_I is increased further, both gears maintain complete contact with each other at all times under the heavy load, therefore the system dynamic response behaves linearly as shown in Figure 8(c).

Next, the role of time varying mesh stiffness on the frequency response is examined as shown in Figure 9 given T_I=0.4. As the degree of time-variation in the mesh stiffness increases, the degree of non-linearity becomes more severe as expected and one begin to see clear effects of super-harmonics below the primary natural frequency of the hypoid gear pair system.

The effect of damping ratio ζ is illustrated in Figure 10. Double-sided impacts are found at low damping values as shown in Figures 10(b) and (c). When ζ is increased to 0.12, double-sided impact case no longer exists, and no impact case and single-sided impact case can define the frequency response completely. The jump-up and jump-down transition frequencies in Figure 10(a) are distinctly apart. With an increase in ζ, the

transition frequencies approach each other, and the jump-up and jump-down transitions in Figure 10(c) take place almost at the same frequency. Similar to the linear system, the increase in damping ratio also lowers the amplitudes in the non-linear resonance regime.

The meshing position and line-of-action vectors for hypoid gears possess time and spatial-varying characteristics. In Figure 11, the effect of time-varying mesh positions and direction of the line-of-action on the gear dynamics is investigated. Figures 11(a) and (b) show the dynamic transmission error spectra predicted using the time-invariant and time-varying mesh vectors under low input load. In Figure 11(c), the time-varying mesh vectors calculated from contact simulation applying CAPP [28] are used. The actual numerical data are given in Appendix B. The results in Figure 11 show that the time-varying mesh characteristic vectors intensify the tooth impacts, and increase the disparity between the responses of the increasing and decreasing rotational speed (mesh frequency). It also affects the jump frequencies and results in an increase in the response amplitude.

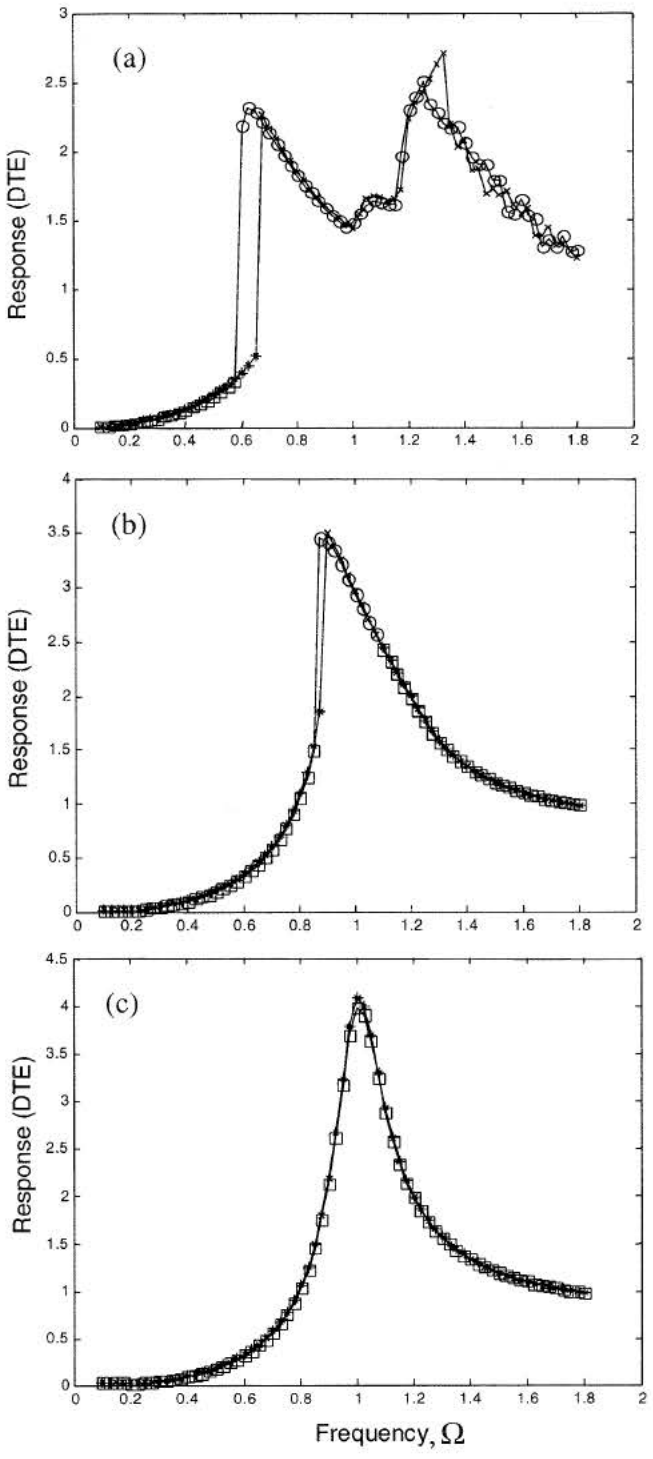

Figure 8. Frequency response for various input load levels for $\tilde{e}_0 = 0.5$, $\varsigma = 0.08$, $k_a = 0.008$: (a) T_1=0.1; (b) T_1=0.4; (c) T_1=0.8. (✳, ×,+: increasing frequency; □, ○, ▽: decreasing frequency. □, ✳, no impact; ○, × , single sided impact; ▽, +, double-sided impact).

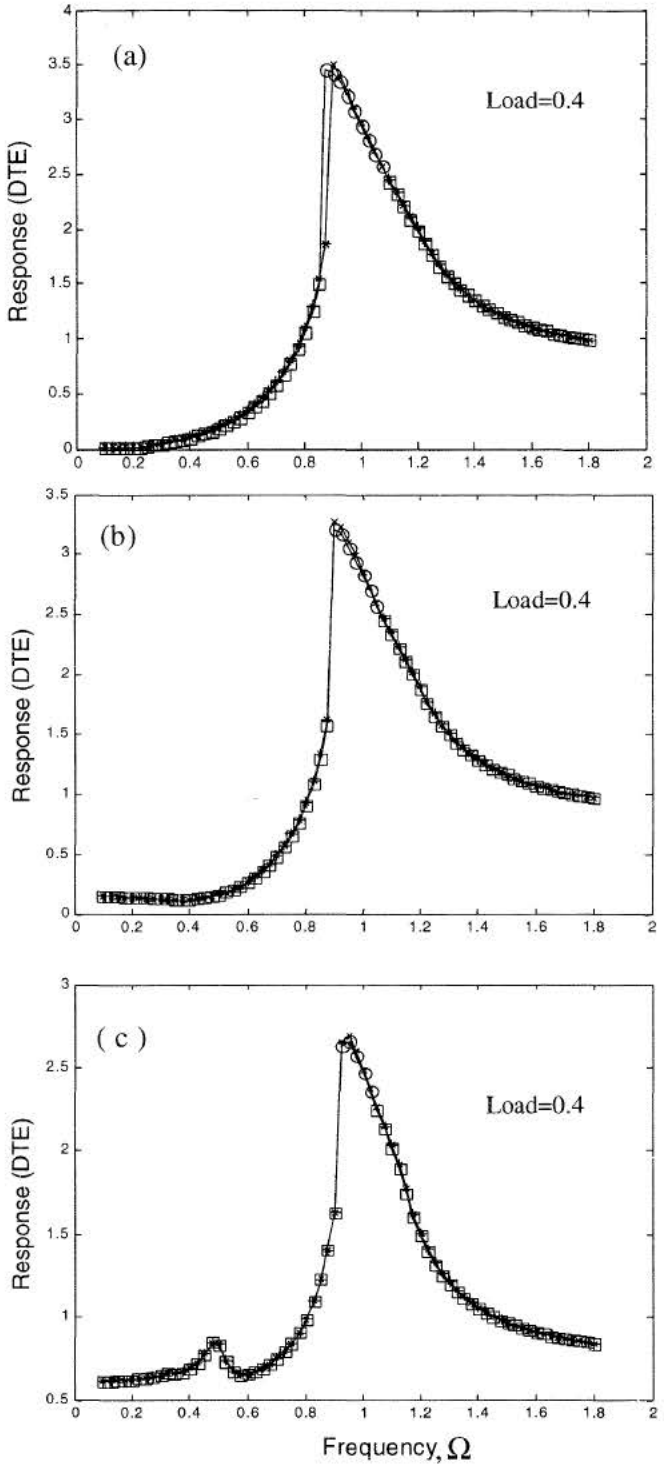

Figure 9. Frequency response for various mesh stiffness variation k_a levels for T_1=0.4, $\tilde{e}_0 = 0.5$, $\varsigma = 0.08$: (a) $k_a = 0.008$; (b) $k_a = 0.08$; (c) $k_a = 0.3$. (✳, ×,+: increasing frequency; □, ○, ▽: decreasing frequency. □, ✳, no impact; ○, × , single sided impact; ▽, +, double-sided impact).

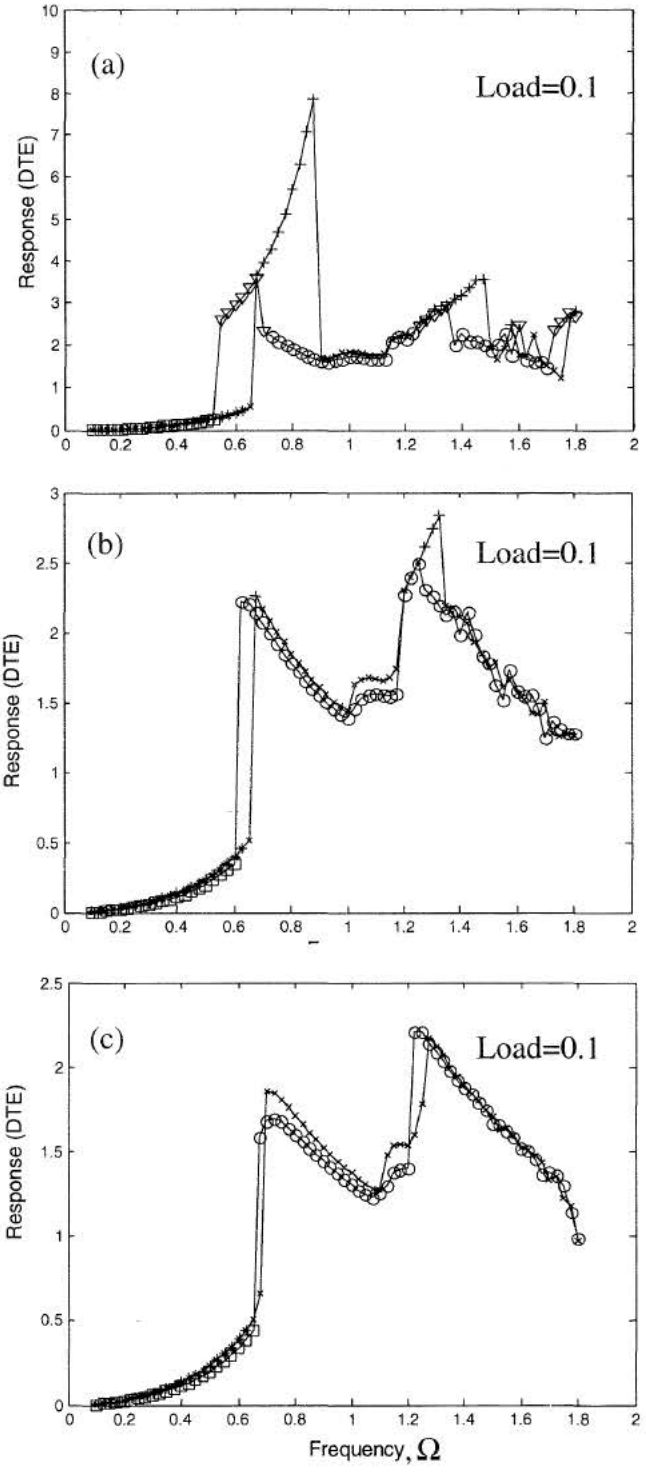

Figure 10. Frequency response for various damping ratios ς with T_1=0.1, $\tilde{e}_0 = 0.5$, $k_a = 0.008$; (a) $\varsigma = 0.04$ (b) $\varsigma = 0.08$; (c) $\varsigma = 0.12$. ($\ast, \times, +$: increasing frequency; $\square, \bigcirc, \bigtriangledown$: decreasing frequency. $\square, \ast$, no impact; $\bigcirc, \times$, single sided impact; $\bigtriangledown, +$, double-sided impact).

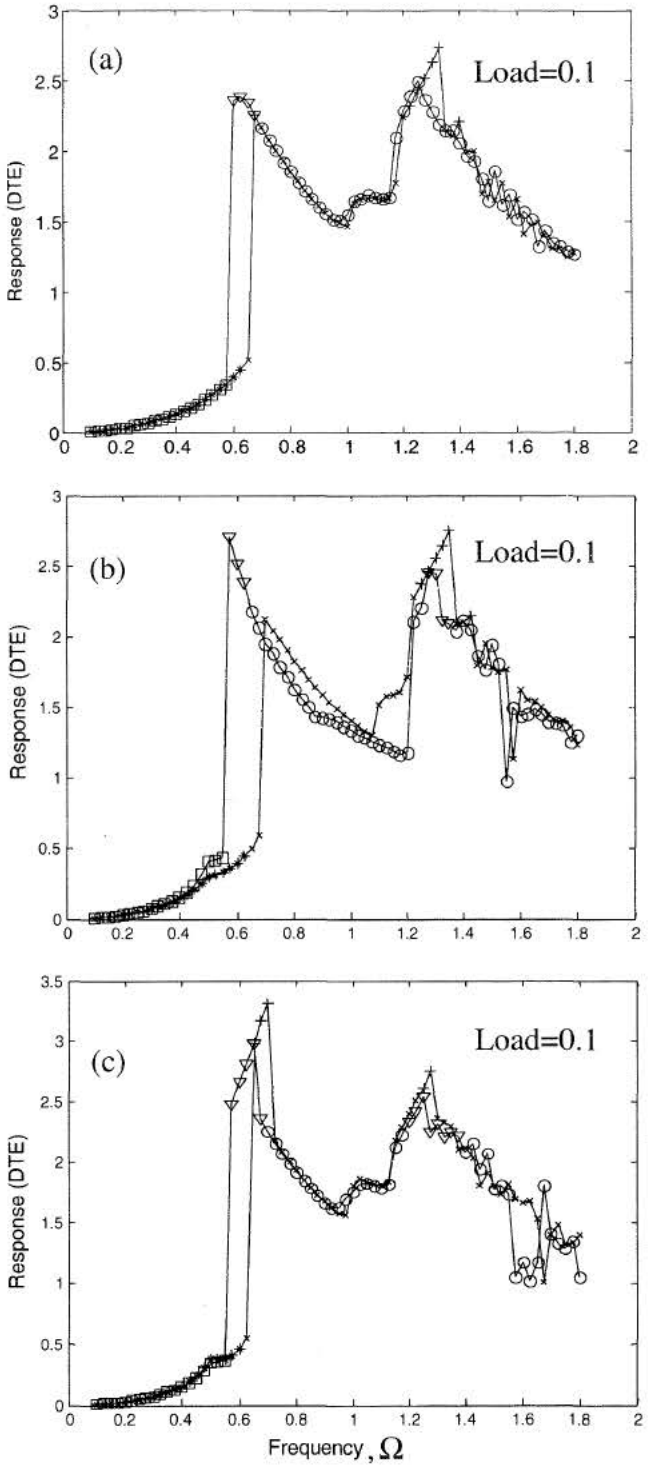

Figure 11. Frequency response for various mesh vector characteristics with T_I=0.1, $\tilde{e}_0 = 0.5$, $k_a = 0.008$: (a) time-invariant mesh vectors; (b) simplified time-varying mesh vectors; (c) time-varying mesh vectors calculated from contact simulation applying CAPP. (✳, ×,+: increasing frequency; □, ○, ▽: decreasing frequency. □, ✳, no impact; ○, ×, single sided impact; ▽, +, double-sided impact).

CHAPTER 5

OUT-OF-PHASE TORSION MODE

5.1. Analytical Solutions

The hypoid gear pair torsional model in the linear case will actually give rise to two modes. These two modes are illustrated in Figure 12. The first mode is a rigid body rotation at essentially zero frequency. The second mode is the out-of-phase torsion mode of the gear pair, which causes a periodic mesh deformation. This mode is believed to be the main contributor to gear noise. This chapter is concerned with the analytical analysis of the out-of-phase system torsion mode.

In hypoid gears, the relative sliding between mating teeth is more uniform and does not reverse direction when the tooth pair passes the pitch point unlike parallel axis gears in which the reversal in sliding friction force causes a shuttling effect. This may allow one to neglect the effect of friction. Assuming that the line-of-action is time-invariant and ignoring the influence of friction, the 2-DOF torsional model can be reduced to a 1-DOF mesh deformation system equation that describes the out-of-phase torsion mode as:

$$\ddot{\tilde{\delta}} + 2\zeta\dot{\tilde{\delta}} + f(\tilde{\delta})\tilde{k}(t) = -\tilde{T}_1 - \tilde{T}_2 - \Omega^2\tilde{e}_0 \sin(\Omega\tau + \phi). \tag{18}$$

The next interest is to develop approximate analytical solutions for the steady-state frequency response of the out-of-phase torsion mode described by equation (18), and to validate the solutions through a comparison with numerical simulation results. A

semi-analytical solution can be constructed by using the harmonic balance method (HBM). The harmonic balance method is iterative in nature, and is based on the assumption that for a given sinusoidal excitation there exists a steady-state solution that can be approximated to satisfactory accuracy using a finite Fourier series.

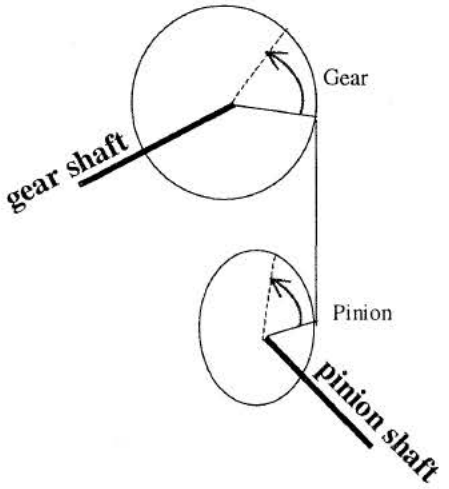

(a) Rigid body (In-phase) gear rotation
($\omega_n = 0Hz$)

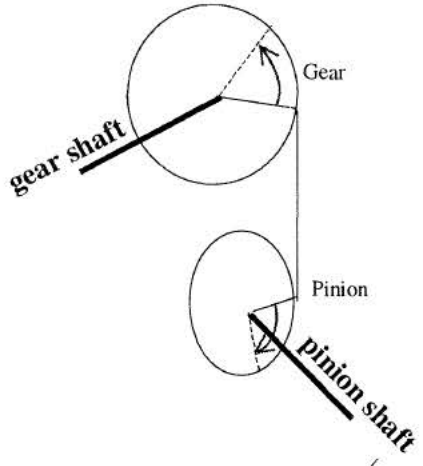

(b) Out-of -phase gear rotation $\left(\omega_n = \sqrt{\frac{K_m}{m_m}} \right)$

Figure 12. Rigid body and flexible torsional modes of the hypoid gear pair.

The harmonic balance method is chosen because this method is well suited to the study of non-linearities described by non-analytic functions. The analysis will consider the non-linear stiffness given by a two-stage symmetric, clearance non-linearity function, linear viscous damping, an internal excitation composed of a mean component and a single frequency alternating component, and the steady-state frequency response associated with the primary resonance only.

The following analytical analysis is performed to focus on steady-state frequency response excited harmonically by the internal transmission error excitation $\tilde{e}_0(t)$ at the normalized mesh frequency Ω. The dimensionless internal force is expressed as $F_i(t) = F_a\Omega^2 \sin(\Omega\tau + \phi)$ with $F_a = \tilde{e}_0 / b$. Defining $F_m = -\tilde{T}_{1g} - \tilde{T}_{2g}$, the governing equation (18) becomes

$$\ddot{\tilde{\delta}} + 2\varsigma\dot{\tilde{\delta}} + f(\tilde{\delta})\tilde{k}(t) = F_m + F_a\Omega^2 \sin(\Omega\tau + \phi). \tag{19}$$

The approximate solution is assumed to have the form of

$$\tilde{\delta}(t) = \tilde{\delta}_m + \tilde{\delta}_a \sin(\Omega\tau + \theta), \tag{20}$$

where $\tilde{\delta}_m$ and $\tilde{\delta}_a$ are the mean and alternating components of the steady-state response, respectively, and θ is the phase angle. The solution given by Equation (20) is based on the assumption that the forced response of Equation (19) is dominated by the first harmonic. Therefore, the higher harmonics and the possibility of super-harmonic or sub-harmonic responses are neglected.

Next, the describing functions theory is introduced into the analysis to quasi-linearize the backlash non-linearity. The quasi-linear approximating functions, which describe approximately the transfer characteristics of the non-linearity, are termed

describing functions. The requirement on the use of describing functions to describe system behavior is that the actual signal at the non-linearity input should approximate the form of signal used to derive the describing functions. For this analysis, the input to the non-linearity is taken to be $F = F_m + F_a\Omega^2 \sin(\Omega\tau + \phi)$. Here, F_m, F_a, and Ω are determined by the nature of the system and its inputs. Thus the only random variable in the characterization of F is the phase angle ϕ, which has the uniform distribution over one cycle. The expectations which appear in the expressions for the describing functions are in this case just single integration over a 2π interval in ϕ. The non-linearity input is the sum of two components: F_m may be taken to be the bias, and $F_a\Omega^2 \sin(\Omega\tau + \phi)$ as the sinusoid. With F_m being a deterministic quantity and the sinusoid $F_a\Omega^2 \sin(\Omega\tau + \phi)$ having zero mean, these two input components are obviously uncorrelated. The output of the optimum quasi-linear approximation to this form of non-linearity can be expressed as

$$f(\tilde{\delta}) = N_m\tilde{\delta}_m + N_a\tilde{\delta}_a \sin(\Omega t + \theta) + N_a^*\tilde{\delta}_a \cos(\Omega t + \theta). \tag{21}$$

The approximate gain to the bias input component is given by

$$N_m = \frac{1}{2\pi\delta_m}\int_0^{2\pi} f(\delta_m + \delta_a \sin\phi)d\phi. \tag{22a}$$

The real and imaginary parts of the complex gain to the sinusoidal input component are given by

$$N_a = \frac{1}{\pi\delta_a}\int_0^{2\pi} f(\delta_m + \delta_a \sin\phi)\sin\phi\, d\phi, \tag{22b}$$

$$N_a^* = \frac{1}{\pi\delta_a}\int_0^{2\pi} f(\delta_m + \delta_a \sin\phi)\cos\phi\, d\phi. \tag{22c}$$

Once the Fourier series expansions for the non-linear functions have been obtained (the describing functions), they are substituted into the original differential equation along with the assumed forms of the solution and the excitation to obtain

$$N_m = 1 + \frac{\tilde{\delta}_a}{2\tilde{\delta}_m}\left[g(\frac{1-\tilde{\delta}_m}{\tilde{\delta}_a}) - g(\frac{-1-\tilde{\delta}_m}{\tilde{\delta}_a}) \right], \tag{23a}$$

$$N_a = 1 - \frac{1}{2}\left[h(\frac{1-\tilde{\delta}_m}{\tilde{\delta}_a}) - h(\frac{-1-\tilde{\delta}_m}{\tilde{\delta}_a}) \right], \tag{23b}$$

$$N_a^* = 0 , \tag{23c}$$

where

$$g(\gamma) = \begin{cases} \frac{2}{\pi}(\gamma \sin^{-1}\gamma + \sqrt{1-\gamma^2}) & |\gamma| \le 1 \\ |\gamma| & |\gamma| > 1 \end{cases}, \tag{23d}$$

$$h(\gamma) = \begin{cases} -1, & \gamma < 1 \\ \frac{2}{\pi}(\sin^{-1}\gamma + \gamma\sqrt{1-\gamma^2}), & |\gamma| \le 1 \\ +1, & \gamma > 1 \end{cases}, \tag{23e}$$

$$\gamma = \frac{\pm 1 - \tilde{\delta}_m}{\delta_a}. \tag{23f}$$

To facilitate the discussion of the existence, uniqueness and general characteristics of the solutions, the functions $g(\gamma)$ and $h(\gamma)$ are replaced by truncated series expansions. The series expansions for the elements of $g(\gamma)$ and $h(\gamma)$ are

$$\sin^{-1}\gamma = \gamma - \frac{\gamma^3}{6} + \frac{3\gamma^5}{40} - \cdots , \qquad \sqrt{(1-\gamma^2)} = 1 - \frac{\gamma^2}{2} - \frac{\gamma^4}{8} + \cdots ,$$

$$\gamma \sin^{-1}\gamma = \gamma^2 - \frac{\gamma^4}{6} + \frac{3\gamma^6}{40} - \cdots, \qquad \gamma\sqrt{(1-\gamma^2)} = \gamma - \frac{\gamma^3}{2} - \frac{\gamma^5}{8} + \cdots.$$

The truncated series expressions are obtained by retaining only the first two terms in each series and adjusting the coefficient of the second term to yield the actual value of the series when the argument $\gamma = 1$. This modification is necessary because when the argument is close to 1, the contribution from the higher terms is significant. For small values of γ, the contribution from the higher terms is small and the modification is not required as these terms have little or no effect on the functions $g(\gamma)$ and $h(\gamma)$. The truncated series that are within 5% of the original function of $g(\gamma)$ and within 6% of $h(\gamma)$ are found to be as follows for $|\gamma| \le 1$:

$$g(\gamma) = \frac{2}{\pi}(1 + (\frac{\pi - 2}{\pi})\gamma^2), \tag{24a}$$

$$h(\gamma) = \frac{4}{\pi}(\gamma - (\frac{4 - \pi}{4})\gamma^3). \tag{24b}$$

Note that these describing functions need to be defined for each impact regime (no impact, single-sided impact, double-sided impact). Governing equations for frequency response are obtained by substituting Equations (12) and (13) into Equation (11), and equating the coefficients of like harmonics. Suppose $\theta = \psi_k$, the closed-form solution is

$$\tilde{\delta}_a = \frac{-b + \sqrt{b^2 - 4ac}}{2a}, \tag{25a}$$

$$\tilde{\delta}_m = \frac{F_m - \frac{1}{2}N_a\tilde{\delta}_a k_a}{N_m}. \tag{25b}$$

$$a = (N_a - \frac{1}{2}N_a k_a^2 - \Omega^2)^2 + 4\varsigma^2\Omega^2, \tag{25c}$$

$$b = 2(N_a - \frac{1}{2}N_a k_a^2 - \Omega^2)F_m k_a, \tag{25d}$$

$$c = -\Omega^4 F_a{}^2. \tag{25e}$$

Since there are 3 possible impact cases depending on ς and F_m, F_a and Ω, multiple solutions are possible and each case is discussed separately below. The combined solutions of all 3 regimes can be used to construct the complete response function.

Case 1: No impact. No tooth separation (impact) is observed if $\tilde{\delta}(t)$ lies in the region $\tilde{\delta}(t)>1$ all the time. This condition is specifically described as

$$\left|\tilde{\delta}_m + \tilde{\delta}_a\right| > 1, \left|\tilde{\delta}_m - \tilde{\delta}_a\right| > 1. \tag{26}$$

It follows that the describing functions are given by

$$N_m = 1 - 1/\tilde{\delta}_m, \tag{27a}$$

$$N_a = 1. \tag{27b}$$

Substitution of Equation (27) into Equation (25) yields the following solutions for no-impact case

$$\tilde{\delta}_a = \frac{-b + \sqrt{b^2 - 4ac}}{2a}, \tag{28a}$$

$$\tilde{\delta}_m = F_m + \frac{1}{2}\tilde{\delta}_a k_a + 1, \tag{28b}$$

$$a = (1 - \frac{1}{2}k_a^2 - \Omega^2)^2 + 4\varsigma^2\Omega^2, \tag{28c}$$

$$b = 2(1 - \frac{1}{2}k_a^2 - \Omega^2)F_m k_a, \tag{28d}$$

$$c = -\Omega^4 F_a{}^2. \tag{28e}$$

Case 2: Single-sided impact. The single-sided impacts (tooth separation without back collision) are observed if

$$\tilde{\delta}_m + \tilde{\delta}_a > 1, \left|\tilde{\delta}_m - \tilde{\delta}_a\right| < 1. \tag{29}$$

The solution remains in the regions of $\tilde{\delta}(t) > -1$, and the corresponding describing functions are derived as

$$N_m = 1 - (\tilde{\delta}_{2a} / 2\tilde{\delta}_{m2})[\gamma_+ - g(\gamma_-)], \tag{30a}$$

$$N_a = 1 - \frac{1}{2}[1 + h(\gamma_-)]. \tag{30b}$$

The solution for the single-sided impact case is obtained by solving Equations (24) and (30) numerically. The validity of the solutions should be checked by examining the conditions defined by Equation (29). If the solution does not satisfy the Equation (29), then single-sided impact will not be seen at that particular frequency.

Case 3: Double-sided impact. Double-sided impact case exists if

$$\tilde{\delta}_a > \left|1 - \tilde{\delta}_m\right|, \ \tilde{\delta}_a > \left|1 + \tilde{\delta}_m\right|. \tag{31}$$

The describing functions and corresponding solutions for this case are

$$N_m = 1 - \frac{2(\pi - 2)}{\pi \tilde{\delta}_{a3}}, \tag{32a}$$

$$N_a = 1 - \frac{4}{\pi}\left[\frac{1}{\tilde{\delta}_{a3}} - \left(\frac{4 - \pi}{4}\right)\left(\frac{1 + 3\tilde{\delta}_{m3}{}^2}{\tilde{\delta}_{a3}{}^3}\right)\right]. \tag{32b}$$

The solution for the double-sided impact case is also obtained by solving Equations (24) and (32) numerically similar to the single-sided case. The validity of the solutions, again, should be checked by examining the conditions defined by Equation (31), as is done in the single-sided impact case.

5.2. Comparison of Analytical and Numerical Solutions

The approximate analytical solutions are validated by comparing the predictions with the results obtained from numerical simulation as shown in Figures 13-15. Effects of load on the frequency response curves of $\tilde{\delta}_a$ versus Ω, and $\tilde{\delta}_m$ versus Ω are generated. All three impact regimes are shown on these plots. First, the lightly loaded system with $\tilde{T}_1$=0.1, $\tilde{e}_0$=0.75 and ς=0.08 is considered as shown in Figure 13. Overall, the numerical and analytical results are very close to each other as both predict the same amplitudes and impact zones. In the frequency range above $\Omega = 1$, the numerical results show sub-harmonic or chaotic response that cannot be obtained using the harmonic balance method. For higher load cases, the numerical and analytical results agree almost exactly as shown in Figures 14 and 15. Also note that the behavior becomes more linear as load increases. Both gears maintain complete contact with each other when $\tilde{T}_1$ is large, say $\tilde{T}_1$=0.8 in Figure 15. Consequently the dynamic system is linear.

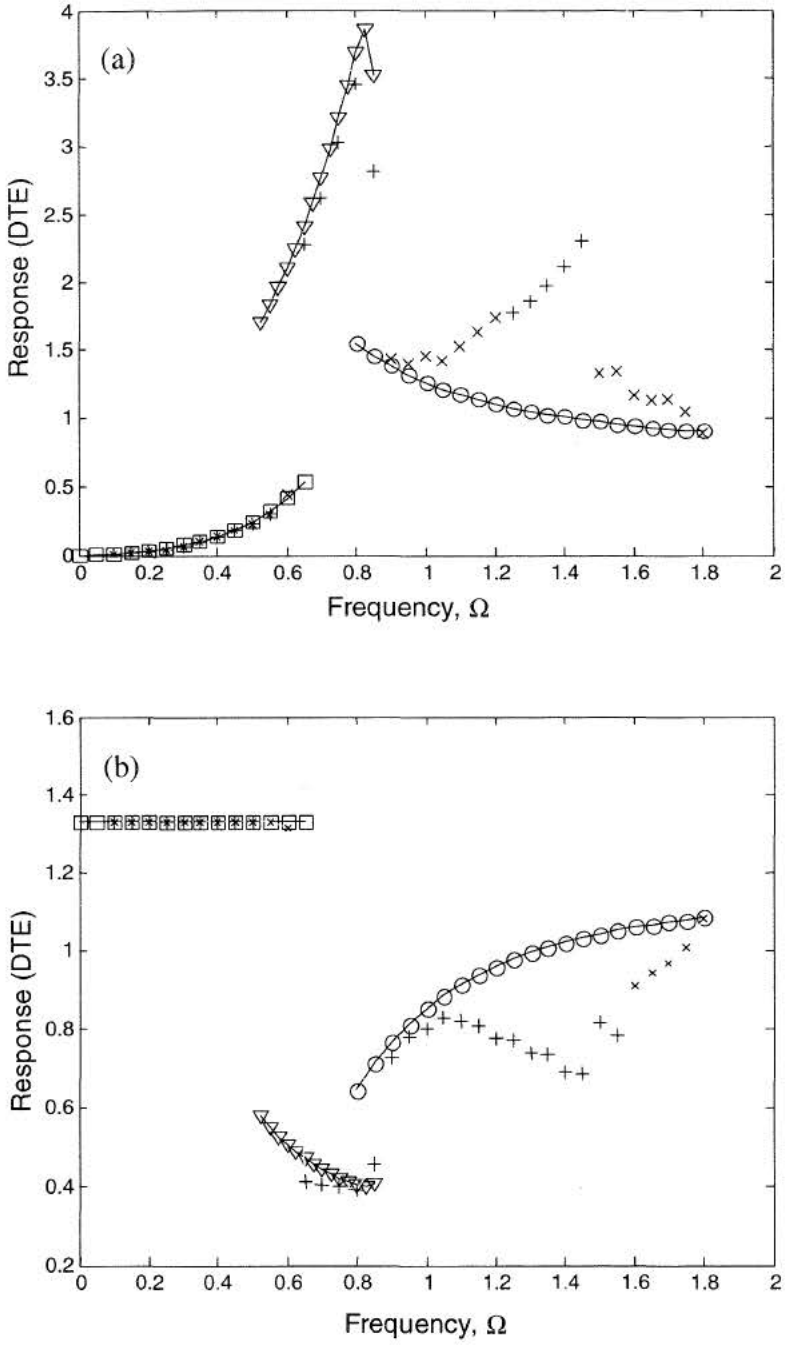

Figure 13. Comparison of analytical results (□, ○, ▽) with numerical simulation (✳, ×,+) for T_1=0.1, $\tilde{e}_0$=0.75, $\varsigma = 0.08$, $k_a = 0.008$: (a) $\tilde{\delta}_a$ versus Ω; (b) $\tilde{\delta}_m$ versus Ω. (□, ✳, no impact; ○, ×, single sided impact; ▽, +, double-sided impact).

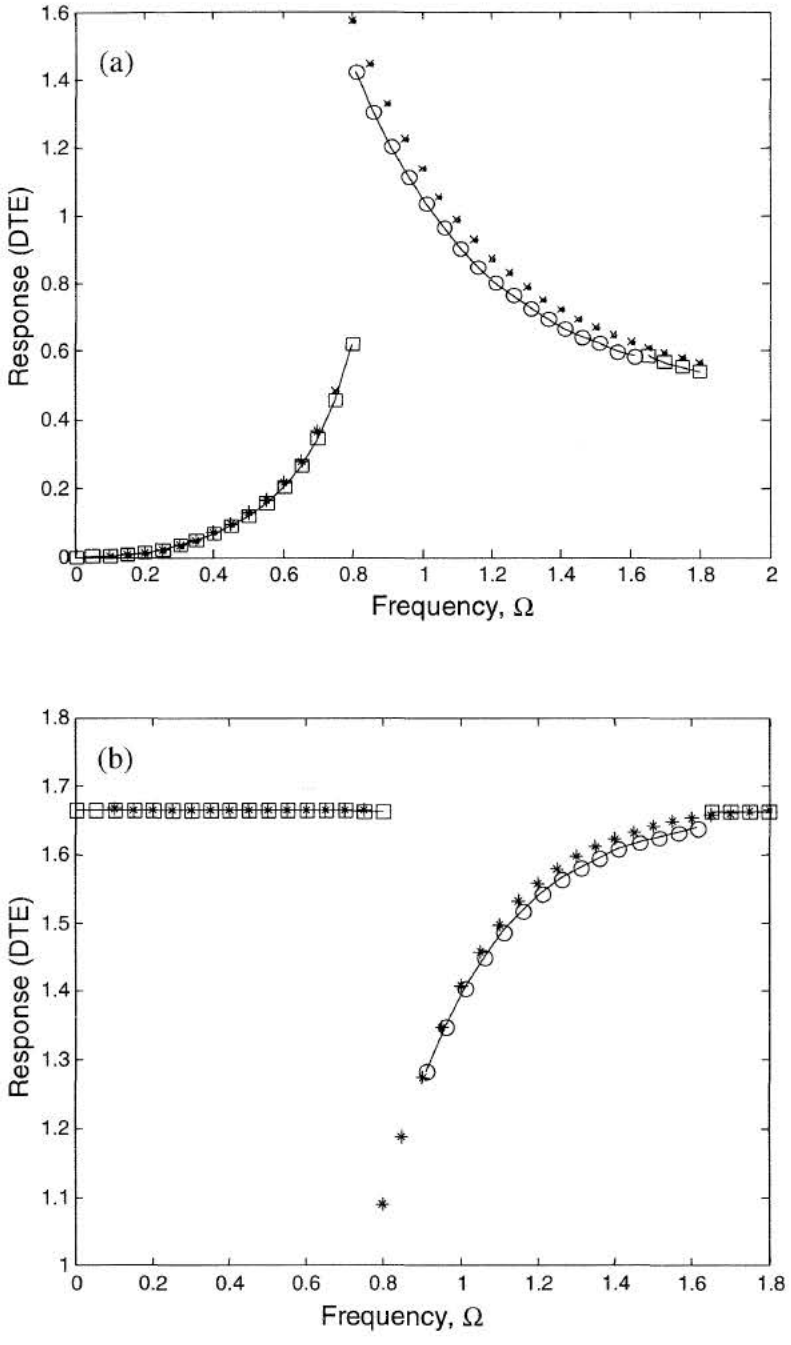

Figure 14. Comparison of analytical results (□, ○, ▽) with numerical simulation (✳, ×,+) for T_1=0.4, $\tilde{e}_0$=0.5, $\varsigma = 0.08$, $k_a = 0.008$: (a) $\tilde{\delta}_a$ versus Ω; (b) $\tilde{\delta}_m$ versus Ω. (□, ✳, no impact; ○, ×, single sided impact; ▽, +, double-sided impact).

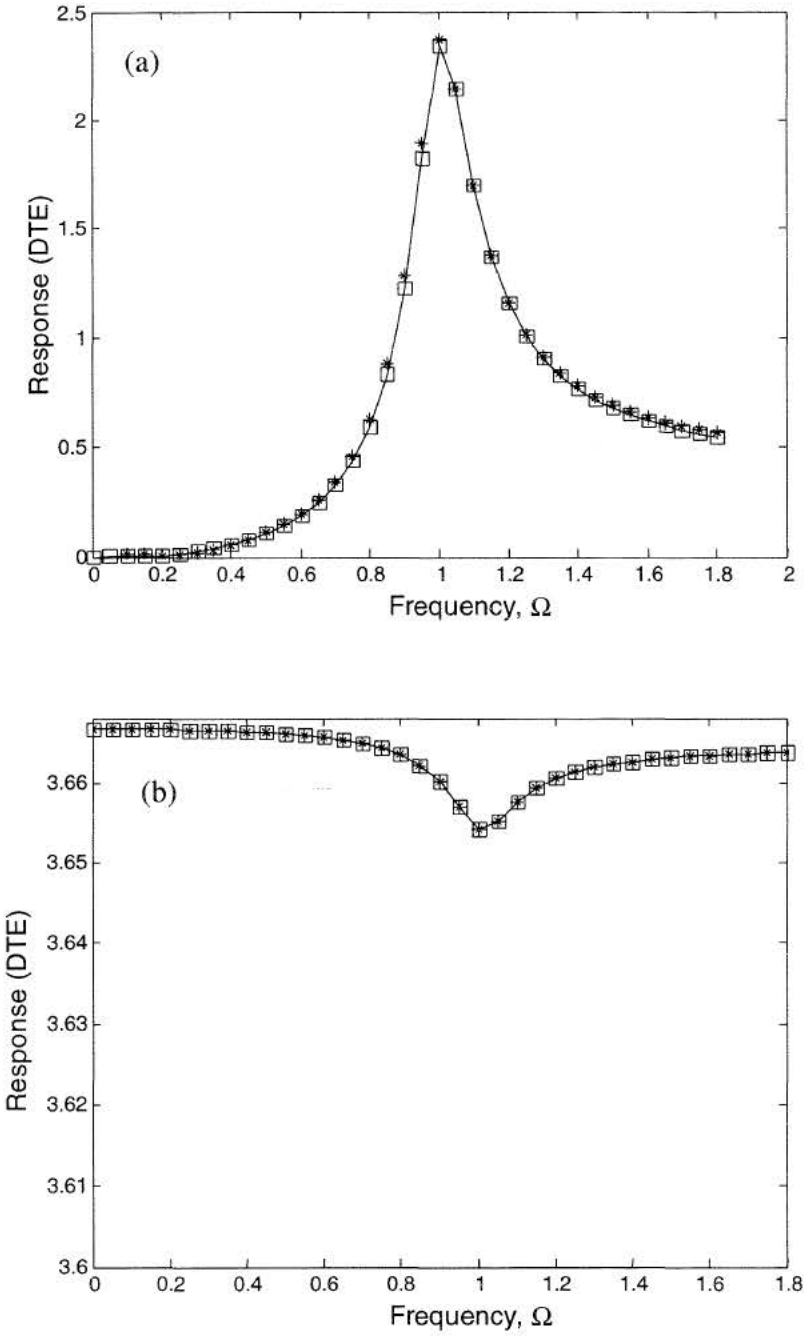

Figure 15. Comparison of analytical results (□, ○, ▽) with numerical simulation (✳, ×,+) for T_1=0.8, $\tilde{e}_0$=0.5, $\varsigma = 0.08$, $k_a = 0.008$: (a) $\tilde{\delta}_a$ versus Ω; (b) $\tilde{\delta}_m$ versus Ω. (□, ✳, no impact; ○, ×, single sided impact; ▽, +, double-sided impact).

CHAPTER 6

NON-LINEAR GEAR DYNAMIC RESPONSE

6.1. Response of Light Load Cases

As discussed previously, non-linear system behaviors are most acute under light load conditions. Because the harmonic balance method is incapable of predicting chaotic and sub-harmonic responses, the numerical simulation technique is employed here to investigate the occurrence of non-linear characteristics such as the jump phenomenon, existence of multiple impact regions, and sub-harmonic and chaotic responses depending on the system parameters and operating conditions.

Figure 16 is a typical system frequency response of the baseline system under mean load T_1=0.1. Note that a jump discontinuity occurs at approximately $\Omega = 0.675$. The time histories around this frequency are shown in Figures 17-20. The dimensionless backlash is from –1 to 1; therefore, impacts occur when dynamic transmission error (DTE) falls within -1 to 1. At $\Omega = 0.625$, DTE always lies below –1 as shown in Figure 17, and hence no tooth separation and no tooth impact occur. At the next frequency $\Omega = 0.65$ in Figure 18, the DTE function wanders slightly into the –1 to 1 region. Hence. single-sided impact occurs here. The amplitudes of the solutions at these two frequencies are still close to each other. When the frequency is increased to 0.675 in Figure 19, the DTE response goes farther across –1 and increases dramatically as well. This sudden

increase in the amplitude of the DTE results in a sudden jump in the frequency response. For $\Omega = 0.7$ in Figure 20, the DTE response is seen close to the response for $\Omega = 0.675$.

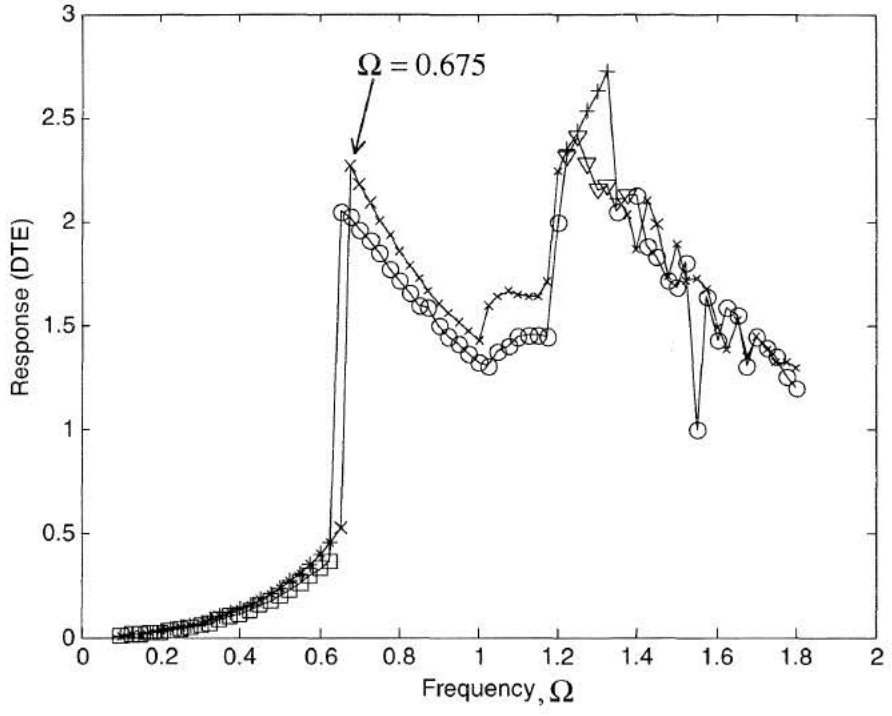

Figure 16. Frequency response of baseline system for mean load T_1=0.1, $\tilde{e}_0$=0.5, $k_a = 0.008$. (✳, ×,+: response for increasing frequency; □, ○, ▽: response for decreasing frequency. □, ✳, no impact; ○, ×, single sided impact; ▽, +, double-sided impact).

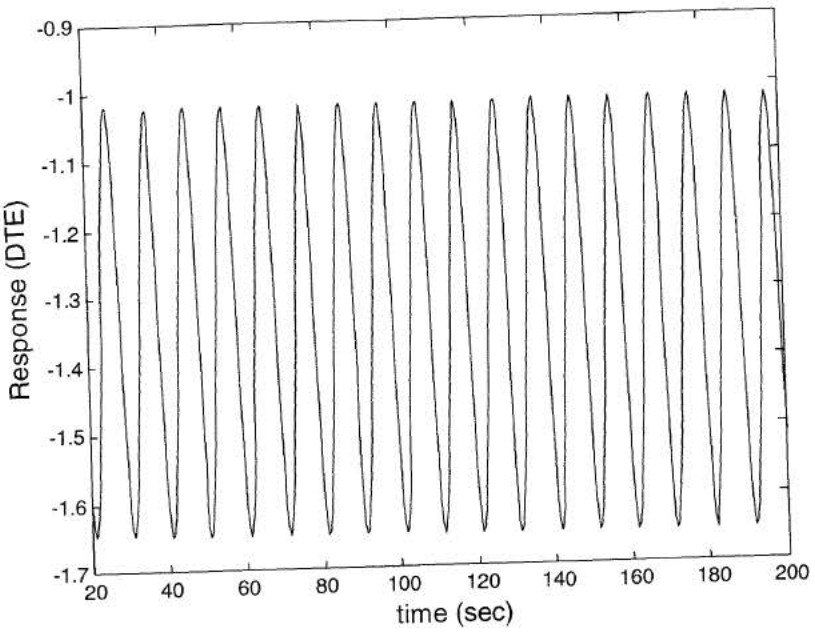

Figure 17. Time history of system steady-state response for $\Omega = 0.625$.

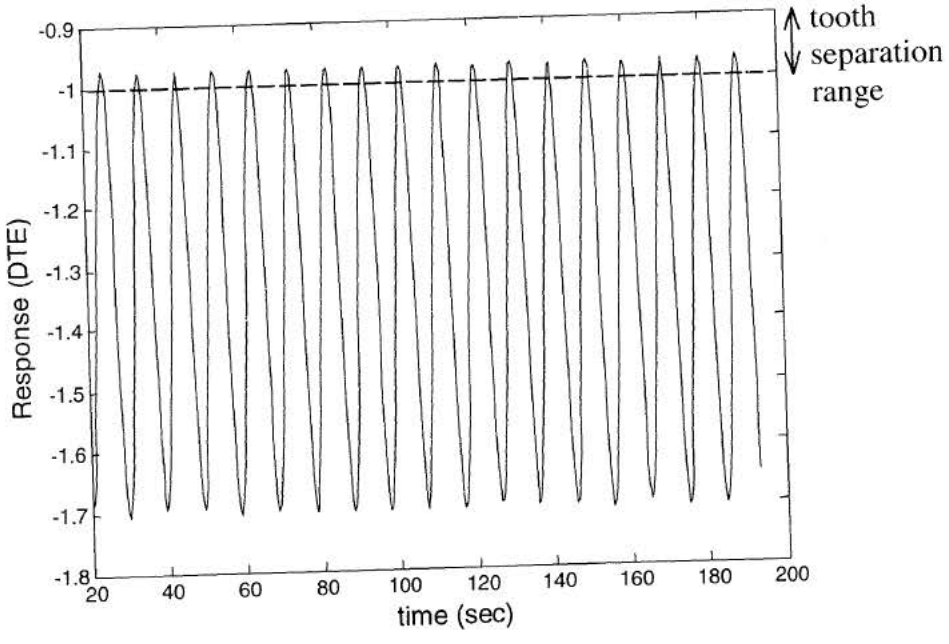

Figure 18. Time history of system steady-state response for $\Omega = 0.65$.

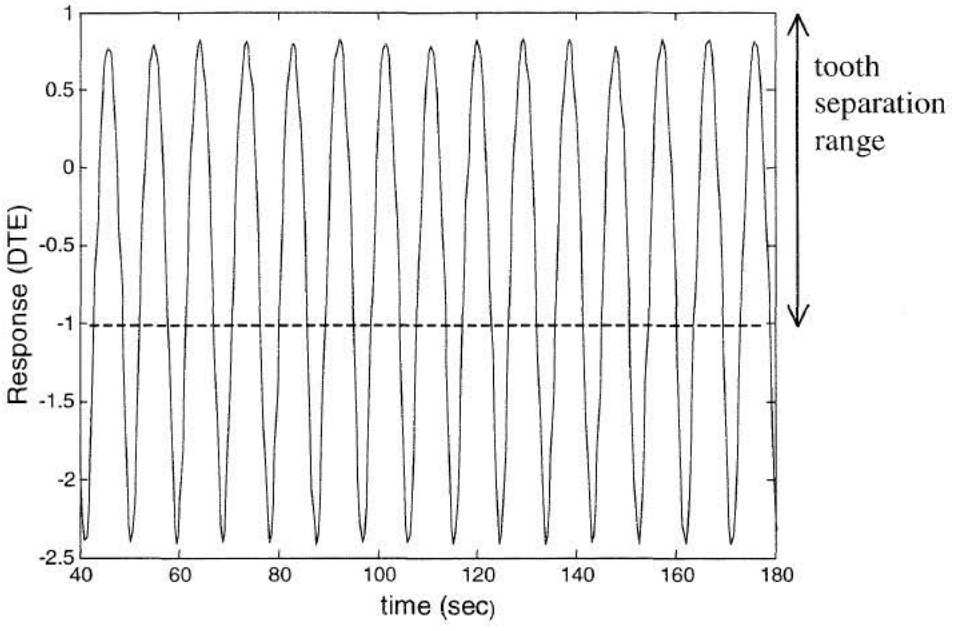

Figure 19. Time history of system steady-state response for $\Omega = 0.675$.

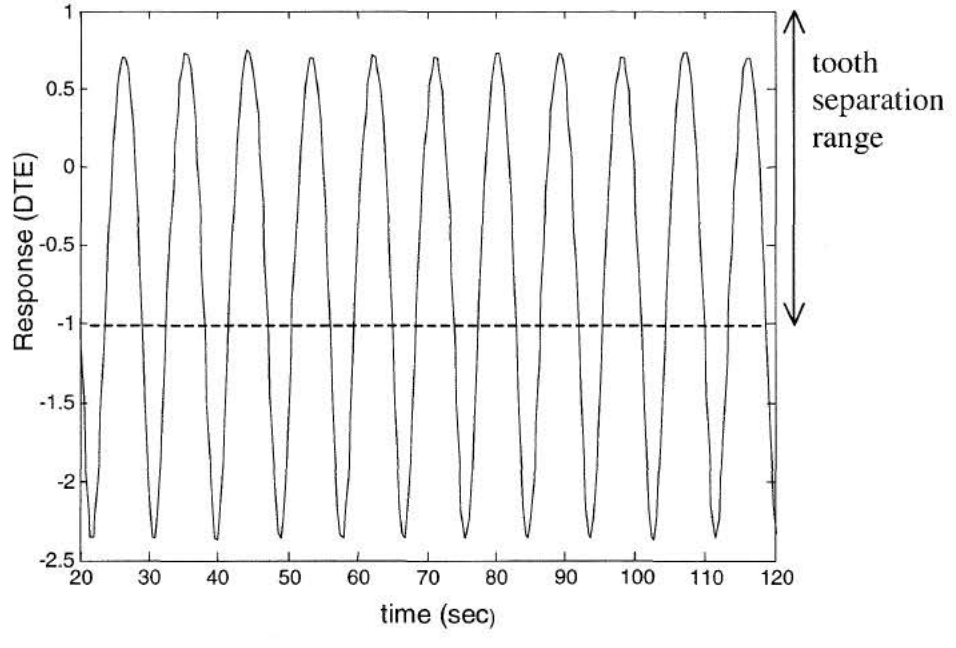

Figure 20. Time history of system steady-state response for $\Omega = 0.7$.

6.2. Classification of Steady-State Solutions

The steady-state response results excited by the transmission error at each mesh frequency Ω can be categorized into the following five classes: (i) harmonic and nearly harmonic solutions at the forcing period of $T = 2\pi / \Omega$ (period-one); (ii) non-harmonic period-one solution; (iii) sub-harmonic solution with period nT, $n > 1$; (iv) quasi-periodic solution; (v) chaotic solution (non-periodic, $n \rightarrow \infty$). The solution classification criteria are based on time histories, phase plane plots, Poincare maps, and Fourier spectra as discussed below.

In Figures 21-26 several types of steady-state solutions obtained for the baseline system are illustrated. In Figure 21, a period-one harmonic solution at the frequency of $\Omega = 0.65$ has an elliptic phase plane plot and repeats itself every period T. In this case, the Poincare map consists of one single point. In Figure 21(d), the FFT spectrum corresponding to the time history given in Figure 21 (c) is shown. It contains peaks at $m\Omega$, where Ω is the fundamental frequency and m is a positive integer. A period-two sub-harmonic solution is obtained when $\Omega = 1$ as shown in Figure 22. The Poincare map consists of two discrete points and the frequency spectrum possesses peaks at $m\Omega/2$. Similarly, a period-two sub-harmonic solution is obtained at $\Omega = 1.3$ as shown in Figure 23. As the frequency increases as shown in Figure 24, the period-two solution is transformed into a period-four sub-harmonic solution at $\Omega = 1.4$ that consists of four discrete points in the Poincare map. The frequency spectrum depicts peaks at $m\Omega/4$. At $\Omega = 1.6$, the steady-state solution becomes chaotic as evident from Figure 25. The sharp peak characteristic seen in harmonic and sub-harmonic solutions is transformed into a broadband form of chaotic solution. At $\Omega = 1.8$, however, the steady-state solution

returns to period-two sub-harmonic solution again as shown in Figure 26. Other types of non-linear behavior such as the non-harmonic period-one solution and quasi-periodic solution are not observed in this set of system response.

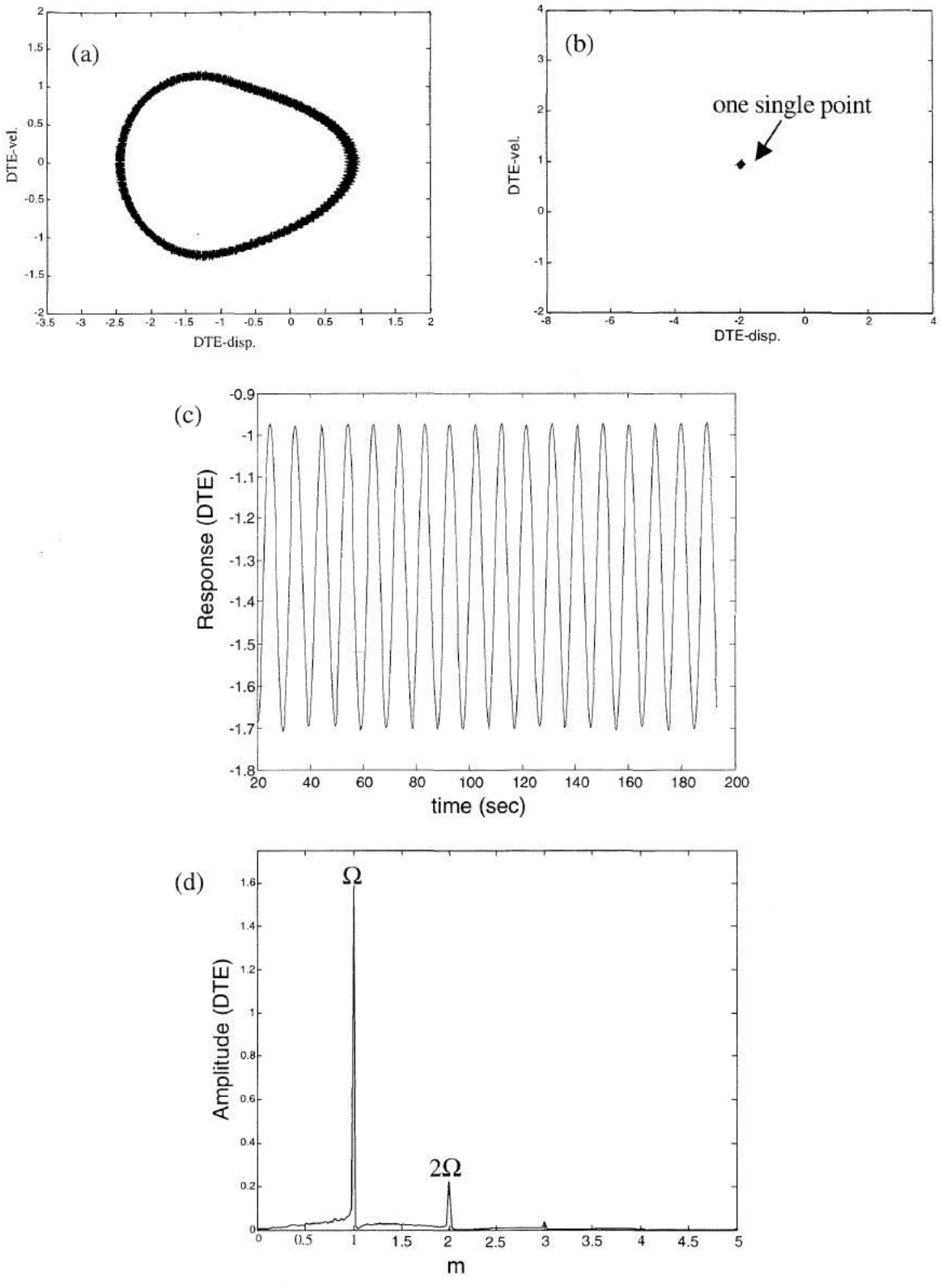

Figure 21. A period-one harmonic response for baseline case, $\Omega = 0.65$; (a) phase plane; (b) Poincare map; (c) time history; (d) FFT spectra.

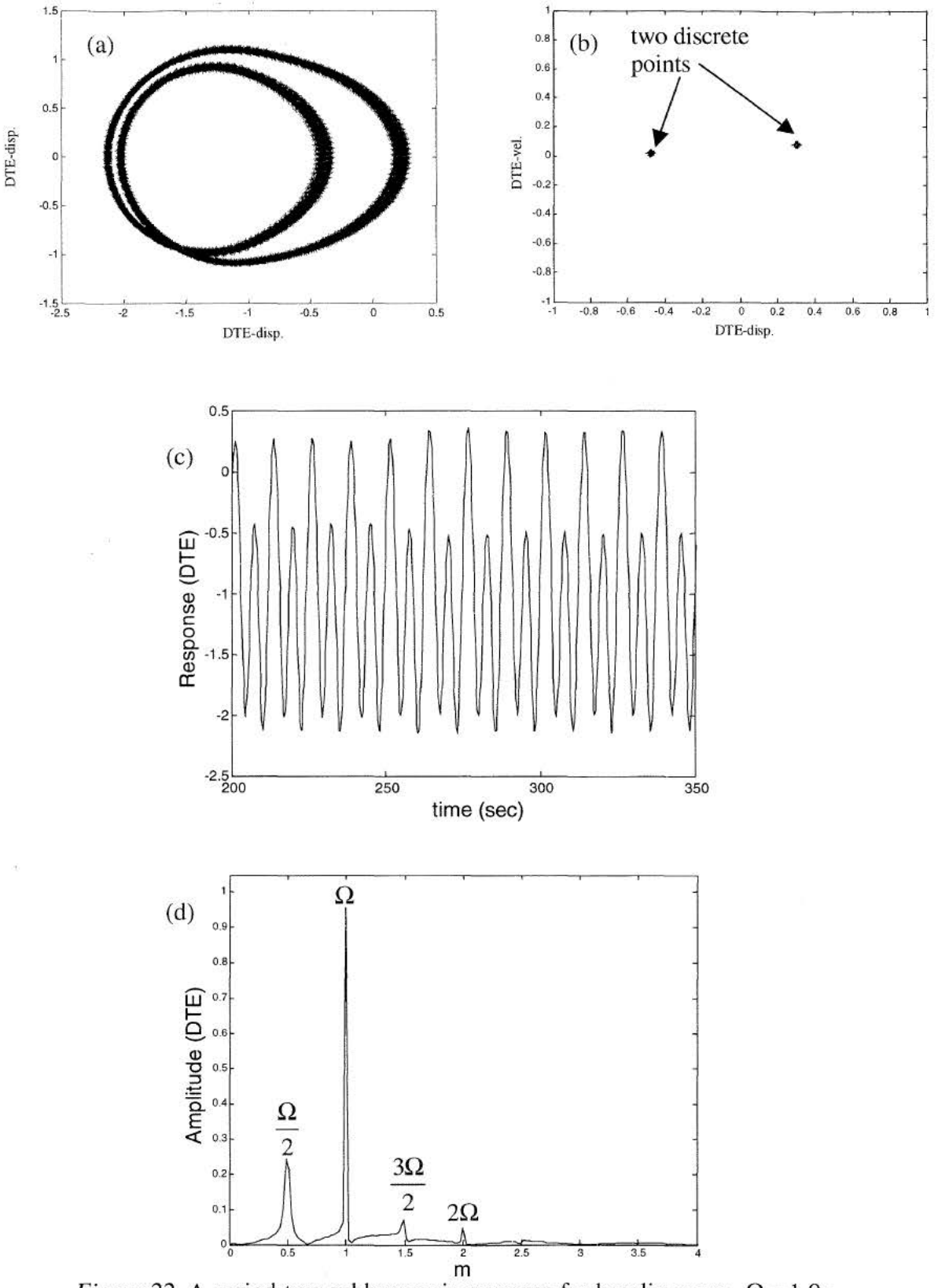

Figure 22. A period-two subharmonic response for baseline case, $\Omega = 1.0$; (a) phase plane; (b) Poincare map; (c) time history; (d) FFT spectra.

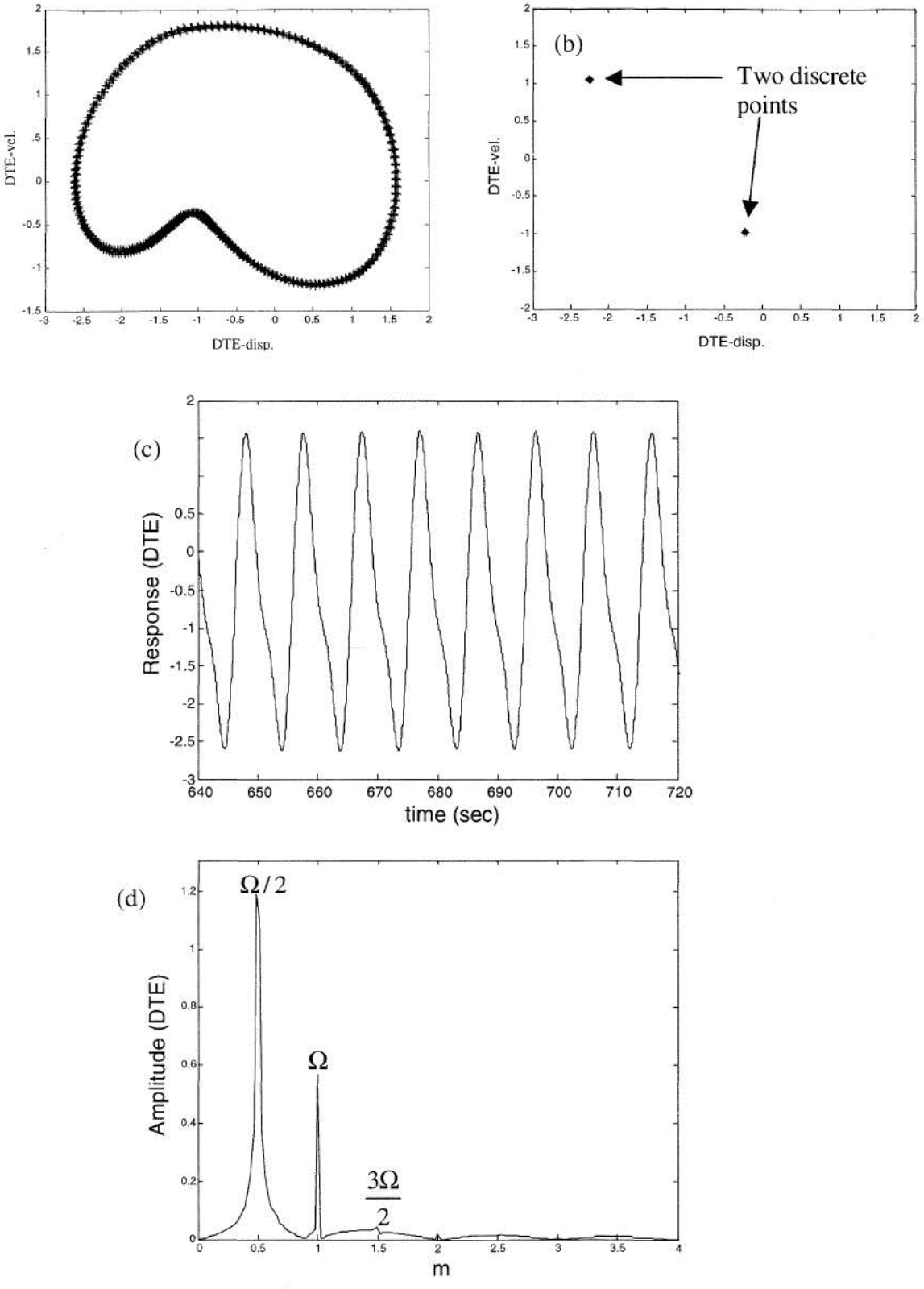

Figure 23. A period-two subharmonic response for baseline case, $\Omega = 1.3$; (a) phase plane; (b) Poincare map; (c) time history; (d) FFT spectra.

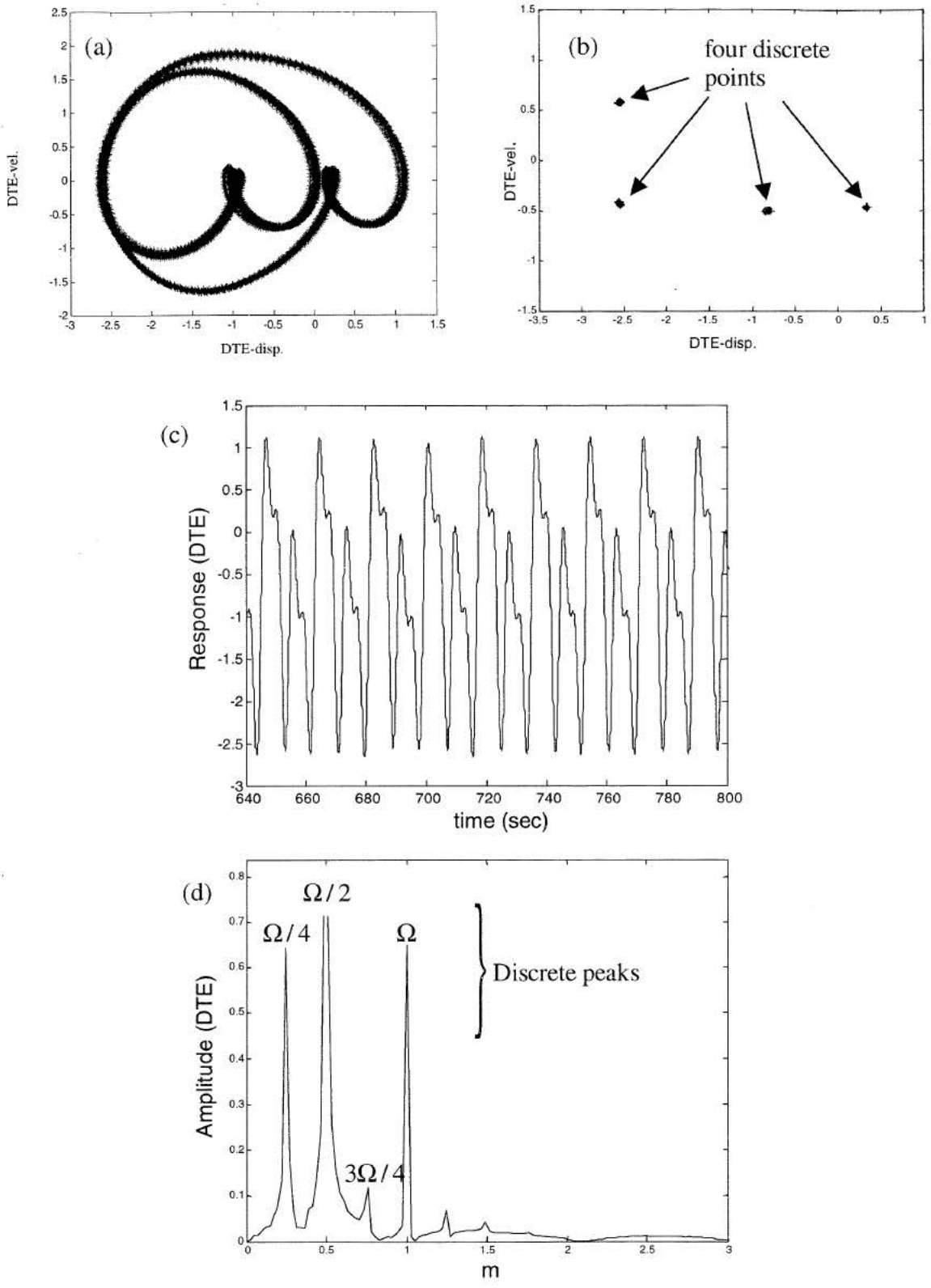

Figure 24. A period-four subharmonic response for baseline case, $\Omega = 1.4$; (a) phase plane; (b) Poincare map; (c) time history; (d) FFT spectra.

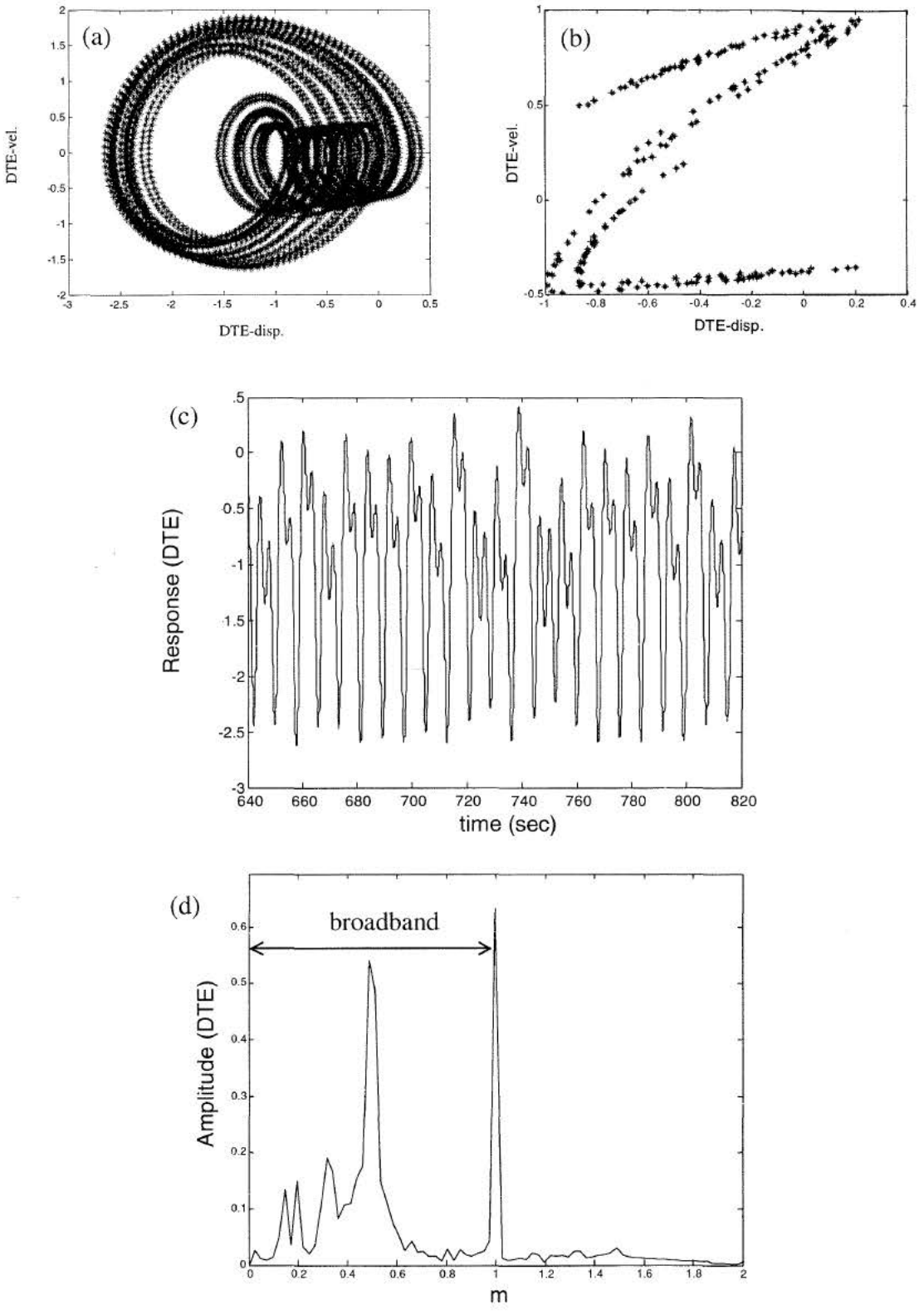

Figure 25. A period-two subharmonic response for baseline case, $\Omega = 1.6$; (a) phase plane; (b) Poincare map; (c) time history; (d) FFT spectra.

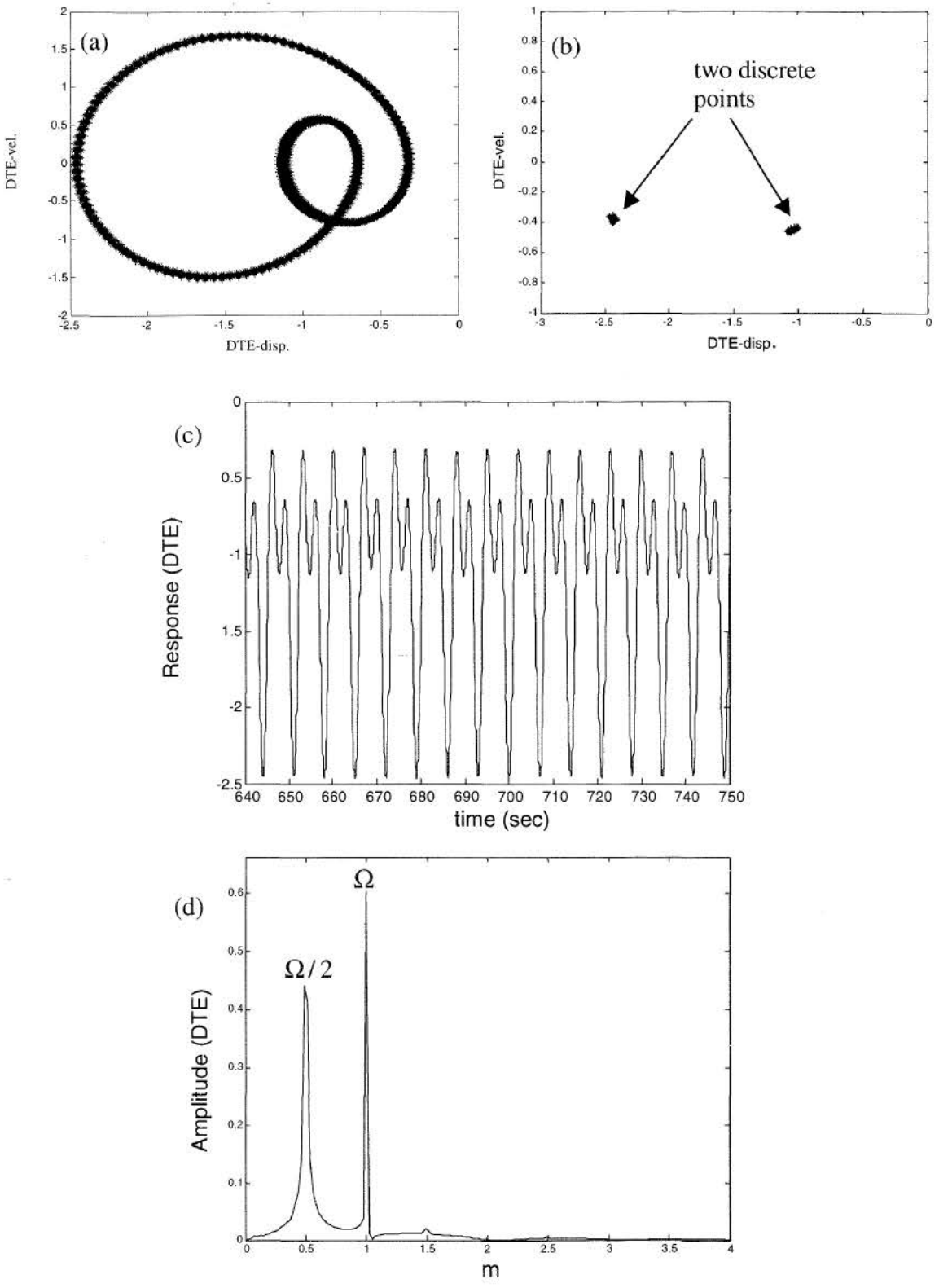

Figure 26. A period-two subharmonic response for baseline case, $\Omega = 1.8$; (a) phase plane; (b) Poincare map; (c) time history; (d) FFT spectra.

CHAPTER 7

CONCLUSIONS AND RECOMMENDATIONS FOR FUTURE WORK

7.1. Concluding Remarks

In this paper, a 2-DOF non-linear time-varying torsional vibration model is developed to simulate the dynamic response of a hypoid gear system. Gear backlash, time-varying mesh characteristic and off line-of-action sliding friction effects are taken into account in this model. Semi-analytical solutions are constructed by using the harmonic balance method. Comparisons of the analytical solutions to numerical integration results show excellent agreement for all load cases. Parametric studies are performed to identify the effects of the controlling factors such as mean load and mesh stiffness variations. Non-linear behavior including jump discontinuities, and chaotic and sub-harmonic resonances are observed in lightly loaded cases. Specifically, the mean load appears to control the conditions for no impact, single-sided impact and double-sided impact. Using the numerical simulation method, the jump discontinuity in the system dynamic response and the onset of tooth impacts are investigated. Based on the time histories, phase plane plots, Poincare maps, and Fourier spectra, the classification of steady-state solutions is accomplished. The current model is developed on the basis of the single-point, gear mesh coupling theory. It can be further refined using a multi-point coupling gear mesh concept, and also extended to examine real-life transmission noise problem.

REFERENCES

1. A. Kahraman, H.N. Ozguven and D.R. Houser. Dynamic analysis of geared rotors by finite elements. *Proceedings of the ASME Power Transmission and Gearing Conference*, Chicago, pp. 375-382, 1989.

2. H.N. Ozguven and D.R. Houser. Dynamic analysis of high speed gears by using loaded transmission error. *Journal of Sound and Vibration*, Vol. 125, No. 1, 1988.

3. H.N. Ozguven and D.R. Houser. Mathematical models in gear dynamics - A review. *Journal of Sound and Vibration*, Vol. 121, No. 3, 1988.

4. A. Kahraman and R. Singh. Linear and non-linear dynamic models of a geared rotor bearing systems. *Proceedings of the 8th International Modal Analysis Conference*, Florida, pp. 697-703, 1990.

5. A. Kahraman and R. Singh. Non-linear dynamics of a spur gear pair. *Journal of Sound and Vibration*, Vol. 142, No. 1, 1990.

6. A. Kahraman and R. Singh. Non-linear dynamics of a geared-rotor bearing system with multiple clearances. *Journal of Sound and Vibration*, Vol. 144, No. 3, 1991.

7. T.C. Lim and R. Singh. Vibration transmission through rolling element bearings. Part III: Geared rotor system studies. *Journal of Sound and Vibration*, Vol. 151, No. 1, 1991.

8. T.C. Lim and R. Singh. A review of gear housing dynamics and acoustics literature. *NASA Contractor Report* 185148, 1989.

9. T.J. Krenzer. Tooth contact analysis of spiral bevel and hypoid gears under load. *SAE Paper* 810688, 1981.

10. M. Sugimoto, I. Nakagawa. Effect of tooth contact and gear dimensions on loaded transmission error of hypoid gears. N. Maruyama and A. Nakayama, *JSAE Print* 882116, 1988.

11. S. Vaidyanathan, H. Busby and D.R. Houser. Rayleigh-Ritz approach to determine compliance and root stresses in spiral bevel gears using shell theory. *AGMA Paper* 93FTM3, 1993.

12. W.D. Mark. The generalized transmission error of spiral bevel gears. *Journal of Mechanisms, Transmissions and Automation in Design*, Vol. 109, 1987.

13. E.W. Newton. Measuring rolling vibrations of hypoid gears. *SAE Paper* 710117, 1971.

14. L.S. Pitts. Bevel and hypoid gear noise reduction. *SAE Paper* 720734, 1972.

15. S. Kiyono. Analysis of vibration of bevel gears. Y. Fujii and Y. Suzuki, *Bulletin JSME*, Vol. 24, 1981.

16. M.G. Donley, T.C. Lim and G.C. Steyer. Dynamic Analysis of Automotive Gearing Systems. *SAE Transactions - Journal of Passenger Cars*, Vol. 101, No. 6, 1992.

17. N. Hirasaka, H. Sugita and M. Asai. A simulation method of rear axle gear noise. *SAE Paper* 911041, 1991.

18. Y. Cheng and Teik C. Lim. Vibration analysis of hypoid transmissions applying an exact geometry-based gear mesh theory. *Journal of Sound and Vibration,* Vol. 240, No. 3, pp. 519-543, 2001.

19. T. C. Lim and Y. Cheng. A theoretical study of the effect of pinion offset on the dynamics of hypoid geared rotor system. *Journal of Mechanical Design*, Vol. 121, No. 4, pp. 594-601, 1999.

20. Y. Cheng and T. C. Lim. Dynamic analysis of high speed hypoid gears with emphasis on automotive axle noise problem. *Proceedings of the ASME Power Transmission and Gearing Conference*, DETC98/PTG-5784, Atlanta, Georgia, 1998.

21. Y. Cheng and T. C. Lim. Dynamics of hypoid gear transmission with time-varying mesh. *Proceedings of the ASME Power Transmission and Gearing Conference*, DETC2000/PTG-14432, Baltimore, Maryland, 2000.

22. Y. Cheng. Dynamics of high-speed hypoid and bevel geared rotor systems. Ph.D. Dissertation, The Ohio State University, 2000.

23. N. Kryloff and N. Bogoliuboff. Introduction to non-linear mechanics. Princeton, Princeton University Press; London, H. Milford, Oxford University Press, 1943.

24. R. J. Comparin and R.Singh. Non-linear frequency response characteristics of an impact pair. *Journal of Sound and Vibration*, Vol. 134, No. 2, pp. 259-290, 1989.

25. R. J. Comparin and R. Singh. Frequency response characteristics of a multi-degree-of-freedom system with clearances. *Journal of Sound and Vibration*, Vol. 142, No. 1, pp.101-124, 1990.

26. A. Kahraman and G. W. Blankenship. Experiments on nonlinear dynamic behavior of an oscillator with clearance and periodically time-varying parameters. *Journal of Applied Mechanics* Mar. Vol. 217, No. 64, 1997

27. M. Vaishya and R. Singh. Sliding Friction-induced non-linearity and parametric effects in gear dynamics. *Journal of Sound and Vibration*, Vol. 248, No. 4, pp. 671-694, 2001.

28. H. B. Wang. Hypoid gear mesh simulation and dynamics. Ph.D. Dissertation, The University of Alabama, 2002.

APPENDIX A

THE FLOW CHART OF THE RUNGE-KUTTA INTEGRATION SCHEME

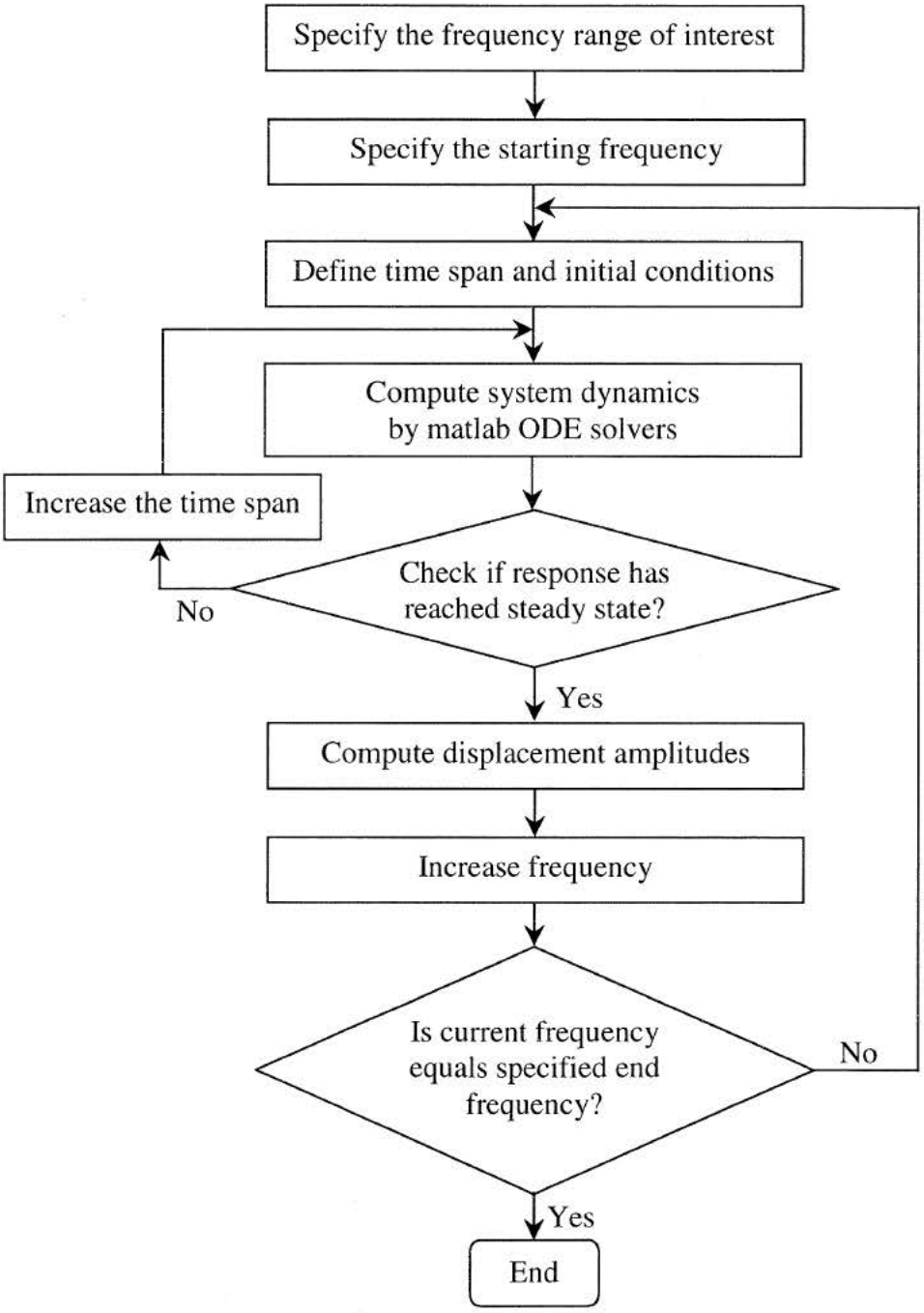

APPENDIX B

MESH VECTORS DATA FROM CONTACT SIMULATION APPLYING CAPP [28]

B.1 Line-of-action (directional cosine unit vectors)

Pinion rotational angle (degree)	X	Y	Z
0	-1.80E-01	-7.55E-01	-6.30E-01
1.125	-1.79E-01	-7.55E-01	-6.31E-01
2.25	-1.77E-01	-7.55E-01	-6.31E-01
3.375	-1.77E-01	-7.54E-01	-6.32E-01
4.5	-1.75E-01	-7.54E-01	-6.33E-01
5.625	-1.74E-01	-7.54E-01	-6.34E-01
6.75	-1.73E-01	-7.53E-01	-6.35E-01
7.875	-1.72E-01	-7.53E-01	-6.35E-01
9.000	-1.71E-01	-7.52E-01	-6.37E-01
10.125	-1.71E-01	-7.51E-01	-6.38E-01
11.25	-1.69E-01	-7.51E-01	-6.38E-01
12.375	-1.68E-01	-7.50E-01	-6.40E-01
13.5	-1.68E-01	-7.50E-01	-6.40E-01
14.625	-1.66E-01	-7.50E-01	-6.40E-01
15.75	-1.65E-01	-7.49E-01	-6.42E-01
16.875	-1.65E-01	-7.48E-01	-6.42E-01
18	-1.63E-01	-7.50E-01	-6.42E-01
19.125	-1.62E-01	-7.49E-01	-6.43E-01
20.25	-1.62E-01	-7.48E-01	-6.43E-01
21.375	-1.59E-01	-7.50E-01	-6.42E-01
22.5	-1.59E-01	-7.49E-01	-6.44E-01
23.625	-1.58E-01	-7.49E-01	-6.44E-01
24.75	-1.55E-01	-7.52E-01	-6.41E-01
25.875	-1.55E-01	-7.49E-01	-6.44E-01
27	-1.55E-01	-7.49E-01	-6.44E-01
28.125	-1.51E-01	-7.53E-01	-6.41E-01
29.25	-1.51E-01	-7.50E-01	-6.44E-01
30.375	-1.52E-01	-7.50E-01	-6.44E-01
31.5	-1.48E-01	-7.54E-01	-6.40E-01
32.625	-1.48E-01	-7.51E-01	-6.44E-01
33.75	-1.49E-01	-7.51E-01	-6.43E-01

34.875	-1.44E-01	-7.56E-01	-6.38E-01
36	-1.44E-01	-7.54E-01	-6.41E-01
37.125	-2.16E-01	-7.59E-01	-6.14E-01
38.25	-2.12E-01	-7.61E-01	-6.13E-01
39.375	-2.11E-01	-7.62E-01	-6.12E-01
40.5	-2.12E-01	-7.60E-01	-6.14E-01
41.625	-2.09E-01	-7.61E-01	-6.14E-01
42.75	-2.08E-01	-7.61E-01	-6.15E-01
43.875	-2.09E-01	-7.59E-01	-6.17E-01
45	-2.06E-01	-7.60E-01	-6.17E-01
46.125	-2.05E-01	-7.60E-01	-6.17E-01
47.25	-2.05E-01	-7.58E-01	-6.19E-01
48.375	-2.03E-01	-7.59E-01	-6.19E-01
49.5	-2.02E-01	-7.59E-01	-6.19E-01
50.625	-2.02E-01	-7.57E-01	-6.21E-01
51.75	-2.00E-01	-7.58E-01	-6.21E-01
52.875	-1.99E-01	-7.58E-01	-6.21E-01
54	-1.99E-01	-7.57E-01	-6.23E-01
55.125	-1.97E-01	-7.57E-01	-6.23E-01
56.2	-1.96E-01	-7.57E-01	-6.24E-01
57.375	-1.95E-01	-7.56E-01	-6.24E-01
58.5	-1.94E-01	-7.56E-01	-6.25E-01
59.625	-1.93E-01	-7.56E-01	-6.25E-01
60.75	-1.92E-01	-7.56E-01	-6.26E-01
61.875	-1.91E-01	-7.55E-01	-6.27E-01
63	-1.89E-01	-7.56E-01	-6.27E-01
64.125	-1.88E-01	-7.56E-01	-6.27E-01
65.25	-1.87E-01	-7.55E-01	-6.28E-01
66.375	-1.86E-01	-7.56E-01	-6.28E-01
67.5	-1.84E-01	-7.56E-01	-6.28E-01
68.625	-1.84E-01	-7.55E-01	-6.29E-01
69.75	-1.82E-01	-7.55E-01	-6.29E-01
70.875	-1.81E-01	-7.56E-01	-6.29E-01
72	-1.80E-01	-7.55E-01	-6.30E-01
73.125	-1.44E-01	-7.54E-01	-6.41E-01
74.25	-1.47E-01	-7.52E-01	-6.42E-01

B.2 Effective mesh contact point (relative to pinion coordinate system S_1)

Pinion rotational angle (degree)	X	Y	Z
0	-4.17E-02	9.79E-03	-1.94E-04
1.125	-4.16E-02	1.02E-02	6.08E-05
2.25	-4.17E-02	1.08E-02	2.38E-04
3.375	-4.16E-02	1.12E-02	5.45E-04
4.5	-4.15E-02	1.17E-02	8.06E-04
5.625	-4.14E-02	1.21E-02	1.08E-03
6.75	-4.13E-02	1.25E-02	1.41E-03
7.875	-4.13E-02	1.30E-02	1.67E-03
9.000	-4.12E-02	1.34E-02	1.99E-03
10.125	-4.11E-02	1.38E-02	2.33E-03
11.25	-4.11E-02	1.43E-02	2.57E-03
12.375	-4.09E-02	1.46E-02	2.92E-03
13.5	-4.08E-02	1.50E-02	3.25E-03
14.625	-4.08E-02	1.56E-02	3.46E-03
15.75	-4.07E-02	1.59E-02	3.82E-03
16.875	-4.07E-02	1.64E-02	4.14E-03
18	-4.07E-02	1.70E-02	4.29E-03
19.125	-4.06E-02	1.74E-02	4.63E-03
20.25	-4.05E-02	1.78E-02	4.97E-03
21.375	-4.07E-02	1.85E-02	5.03E-03
22.5	-4.05E-02	1.88E-02	5.44E-03
23.625	-4.05E-02	1.92E-02	5.75E-03
24.75	-4.08E-02	2.01E-02	5.67E-03
25.875	-4.05E-02	2.03E-02	6.21E-03
27	-4.05E-02	2.07E-02	6.52E-03
28.125	-4.08E-02	2.16E-02	6.41E-03
29.25	-4.05E-02	2.18E-02	6.98E-03
30.375	-4.05E-02	2.22E-02	7.32E-03
31.5	-4.08E-02	2.31E-02	7.13E-03
32.625	-4.05E-02	2.33E-02	7.73E-03
33.75	-4.05E-02	2.36E-02	8.15E-03
34.875	-4.10E-02	2.48E-02	7.74E-03
36	-4.07E-02	2.50E-02	8.31E-03
37.125	-4.20E-02	-5.36E-03	-6.14E-03
38.25	-4.21E-02	-4.51E-03	-6.36E-03
39.375	-4.24E-02	-3.86E-03	-6.30E-03
40.5	-4.22E-02	-3.68E-03	-5.81E-03
41.625	-4.22E-02	-3.05E-03	-5.81E-03
42.75	-4.22E-02	-2.54E-03	-5.64E-03
43.875	-4.20E-02	-2.30E-03	-5.22E-03
45	-4.21E-02	-1.64E-03	-5.23E-03
46.125	-4.22E-02	-1.13E-03	-5.06E-03
47.25	-4.20E-02	-8.34E-04	-4.68E-03

48.375	-4.20E-02	-2.36E-04	-4.63E-03
49.5	-4.21E-02	2.69E-04	-4.45E-03
50.625	-4.19E-02	5.80E-04	-4.09E-03
51.75	-4.20E-02	1.14E-03	-3.99E-03
52.875	-4.20E-02	1.65E-03	-3.82E-03
54	-4.19E-02	1.99E-03	-3.49E-03
55.125	-4.18E-02	2.51E-03	-3.34E-03
56.2	-4.19E-02	3.03E-03	-3.18E-03
57.375	-4.18E-02	3.46E-03	-2.91E-03
58.5	-4.18E-02	3.92E-03	-2.71E-03
59.625	-4.18E-02	4.46E-03	-2.56E-03
60.75	-4.18E-02	4.92E-03	-2.33E-03
61.875	-4.18E-02	5.37E-03	-2.09E-03
63	-4.18E-02	5.93E-03	-1.96E-03
64.125	-4.18E-02	6.41E-03	-1.74E-03
65.25	-4.17E-02	6.81E-03	-1.45E-03
66.375	-4.18E-02	7.39E-03	-1.33E-03
67.5	-4.18E-02	7.90E-03	-1.14E-03
68.625	-4.17E-02	8.29E-03	-8.32E-04
69.75	-4.17E-02	8.82E-03	-6.57E-04
70.875	-4.18E-02	9.38E-03	-4.95E-04
72	-4.17E-02	9.79E-03	-1.96E-04
73.125	-4.07E-02	2.50E-02	8.31E-03
74.25	-4.06E-02	2.51E-02	8.95E-03

B.3 Effective mesh contact point (relative to gear coordinate system S_2)

Pinion rotational angle (degree)	X	Y	Z
0	1.40E-01	6.28E-03	-3.19E-02
1.125	1.40E-01	6.23E-03	-3.17E-02
2.25	1.41E-01	6.26E-03	-3.15E-02
3.375	1.41E-01	6.17E-03	-3.12E-02
4.5	1.42E-01	6.11E-03	-3.09E-02
5.625	1.42E-01	6.04E-03	-3.07E-02
6.75	1.43E-01	5.93E-03	-3.03E-02
7.875	1.43E-01	5.89E-03	-3.01E-02
9.000	1.44E-01	5.77E-03	-2.98E-02
10.125	1.44E-01	5.67E-03	-2.94E-02
11.25	1.45E-01	5.65E-03	-2.92E-02
12.375	1.45E-01	5.51E-03	-2.88E-02
13.5	1.45E-01	5.43E-03	-2.85E-02
14.625	1.46E-01	5.44E-03	-2.83E-02
15.75	1.46E-01	5.29E-03	-2.79E-02
16.875	1.47E-01	5.25E-03	-2.76E-02
18	1.47E-01	5.33E-03	-2.75E-02

19.125	1.48E-01	5.21E-03	-2.71E-02
20.25	1.48E-01	5.14E-03	-2.68E-02
21.375	1.49E-01	5.30E-03	-2.67E-02
22.5	1.49E-01	5.13E-03	-2.63E-02
23.625	1.49E-01	5.11E-03	-2.60E-02
24.75	1.50E-01	5.39E-03	-2.61E-02
25.875	1.51E-01	5.11E-03	-2.55E-02
27	1.51E-01	5.11E-03	-2.52E-02
28.125	1.52E-01	5.39E-03	-2.53E-02
29.25	1.52E-01	5.10E-03	-2.48E-02
30.375	1.52E-01	5.10E-03	-2.44E-02
31.5	1.53E-01	5.43E-03	-2.46E-02
32.625	1.54E-01	5.12E-03	-2.40E-02
33.75	1.54E-01	5.10E-03	-2.36E-02
34.875	1.55E-01	5.60E-03	-2.40E-02
36	1.55E-01	5.32E-03	-2.34E-02
37.125	1.25E-01	6.60E-03	-3.79E-02
38.25	1.26E-01	6.74E-03	-3.81E-02
39.375	1.26E-01	6.99E-03	-3.80E-02
40.5	1.27E-01	6.76E-03	-3.76E-02
41.625	1.27E-01	6.77E-03	-3.76E-02
42.75	1.28E-01	6.83E-03	-3.74E-02
43.875	1.28E-01	6.62E-03	-3.70E-02
45	1.29E-01	6.71E-03	-3.70E-02
46.125	1.29E-01	6.76E-03	-3.68E-02
47.25	1.29E-01	6.59E-03	-3.64E-02
48.375	1.30E-01	6.64E-03	-3.64E-02
49.5	1.31E-01	6.68E-03	-3.62E-02
50.625	1.31E-01	6.52E-03	-3.58E-02
51.75	1.31E-01	6.55E-03	-3.57E-02
52.875	1.32E-01	6.58E-03	-3.56E-02
54	1.32E-01	6.45E-03	-3.52E-02
55.125	1.33E-01	6.44E-03	-3.51E-02
56.2	1.33E-01	6.49E-03	-3.49E-02
57.375	1.34E-01	6.44E-03	-3.47E-02
58.5	1.34E-01	6.39E-03	-3.45E-02
59.625	1.35E-01	6.44E-03	-3.43E-02
60.75	1.35E-01	6.43E-03	-3.41E-02
61.875	1.36E-01	6.36E-03	-3.38E-02
63	1.36E-01	6.42E-03	-3.37E-02
64.125	1.37E-01	6.42E-03	-3.35E-02
65.25	1.37E-01	6.32E-03	-3.32E-02
66.375	1.38E-01	6.39E-03	-3.31E-02
67.5	1.38E-01	6.42E-03	-3.29E-02
68.625	1.39E-01	6.30E-03	-3.26E-02
69.75	1.39E-01	6.33E-03	-3.24E-02
70.875	1.40E-01	6.38E-03	-3.22E-02
72	1.40E-01	6.28E-03	-3.19E-02
73.125	1.55E-01	5.32E-03	-2.34E-02
74.25	1.55E-01	5.16E-03	-2.28E-02